Appendix A: Spectroscopy of CH_3NCO

Thorough analysis of the rotational spectrum of a target molecule is a crucial step that enables astrophysical detection. In the case of CH_3NCO the understanding of the rotational spectrum, and thus delivery of suitable line lists for astrophysical use has been considerably delayed by the complications arising from the presence of two large amplitude internal motions in this molecule. The first laboratory studies were carried out around half a century ago (Curl et al. 1963; Lett et al. 1967) when it was found that the molecule has a very low barrier to internal rotation of the methyl group and also a low-frequency bending mode. In the 1980s those studies were greatly extended by Koput (1984, 1986, 1988). His use of Stark spectroscopy allowed the unambiguous assignment of transitions for different values of K. The use of a semi-rigid rotor Hamiltonian and relative intensity considerations allowed the assignment of the vibrational quantum numbers m and v_b. In this way a very self-consistent picture of the complex vibrational energy structure was reached, as already described in connection with Fig. 1. In an investigation contemporary with that of Koput, the electric dipole moment of CH_3NCO was also precisely determined: μ_a = 2.882 (8) D (Kasten & Dreizler 1986).

Further progress in the investigation of the rotational spectrum of methyl isocyanate was achieved as part of this work. In a first stage a practically continuous 117 – 364 GHz of the molecule was recorded by means of the Fast Scanning Submillimeter Spectroscopic Technique (FASSST) developed at The Ohio State University (Petkie et al. 1997; Medvedev et al. 2004). The spectrum was recorded at room-temperature using a commercially available sample. Although the Koput (1986)

analysis was very successful in accounting for the consequences of the large amplitude motions on the rotational spectrum of this molecule, the deviation of the fit to 210 transitions up to $J = 4 \leftarrow 3$ was 3 MHz, which was well in excess of the 0.05 MHz frequency measurement precision of his spectrometer. Furthermore, even a cursory inspection of the FASSST spectrum (see Fig. 1) revealed that it was devoid of easily discernible spectral patterns and that progress in its traditional interpretation would be difficult. We have, therefore, decided to pursue a pragmatic approach to the characterization of this spectrum based on the generic property of rotational spectra, in that evolution of the frequencies of rotational transitions of a given set of quantum numbers can be described by a smooth function in the J quantum number. It was eventually possible to identify over 220 such line sequences and to fit each sequence to within experimental accuracy with a linear rotor-type model using a power series expansion in $J(J + 1)$, as discussed in a preliminary report in 2010 (Kisiel et al. 2010). The separate line sequences were still without a confident K, m, and v_b quantum number assignment. An initial attempt to transfer such assignments from the Koput work by linking sequences in the FASSST region with those below 40 GHz revealed many ambiguities, due to a still considerable region of missing experimental coverage of the rotational spectrum of CH_3NCO.

For this reason, in a second stage of the laboratory part of the present work, the missing 40 – 117 GHz region of the spectrum was covered in Valladolid by using two complementary spectrometers. The 50 – 117 GHz segment of the spectrum was recorded with a harmonic generation spectrometer based on the multiplication of the synthesizer frequency of up to 20 GHz and employing source modulation detection (Daly et al. 2014). The $J = 5 \leftarrow 4$ transition at 41 – 45 GHz was measured with a Stark modulation spectrometer (Daly et al. 2015) at a modulation voltage of 430 V. The sample was synthesized using the method described by Brändström et al. (1974) and in both spectrometers was kept at room temperature and a pressure of 20 μbar. As a result of the combined effort from the participating laboratories we were able to achieve complete room temperature experimental coverage of the rotational spectrum of methyl isocyanate from the lowest $J = 1 \leftarrow 0$ transition up to the $J = 41 \leftarrow 40$ transition centred near 358 GHz. The analysis procedure first involved creating a single spectrum by combining all available experimental spectra. The intensities for the lines measured by Koput are not available so that the < 40 GHz spectral segment was simulated by assuming equal intensity transitions at the reported frequencies. Measurements on this spectrum were then performed with the AABS package for Assignment and Analysis of Broadband Spectra (Kisiel et al. 2005, 2012), which is freely available from the PROSPE website (Kisiel 2001,a). The fits and predictions were made with Pickett's SPCAT/SPFIT program suite (Pickett 1991) and each line sequence required its own dedicated set of analysis files. In the case of explicit asymmetric rotor fits Watson's A-reduced asymmetric rotor Hamiltonian (Watson 1977) was used. The Loomis-Wood type mode for displaying the rotational spectrum (as pioneered for rotational spectroscopy by Winnewisser et al. (1989) and built into the AABS package) was used for graphical assignment of transitions in specific line sequences. Some preliminary results were reported in the middle of last year (Kisiel et al., 2015) and Loomis-Wood plots for several sample transition sequences are reproduced in Fig. A.1. These plots allow the transfer of the Koput assignment to the higher frequency spectrum. We also consider the Koput assignment to be reliable since it was reached using variable voltage Stark modulation spectroscopy, which provides good discrimination between transitions with different values of K according to their different line profiles. Each of these identified line sequences is reproduced by a suitable $J(J+1)$ power series expansion for the rotational energies

$$\begin{aligned} E_{\rm rot} &= BJ(J+1) - D_J J^2(J+1)^2 + H_J J^3(J+1)^3 \\ &\quad + L_J J^4(J+1)^4 + P_J J^5(J+1)^5 + P_{12} J^6(J+1)^6 \\ &\quad + P_{14} J^7(J+1)^7 + P_{16} J^8(J+1)^8 + P_{18} J^9(J+1)^9 \end{aligned} \quad \text{(A.1)}$$

where the length of the expansion and the magnitudes of the expansion parameters B, D_J, H_J, etc., are determined by the interactions and also by the asymmetry contributions affecting the energy levels in question. The required length of the expansion ranges from only three terms to being insufficient even if all nine terms in Eq. A.1 are used. In several rare cases two power expansions were needed to model a line sequence with a particularly complex J dependence, by splitting the sequence into two parts. The results of such fits for the key assigned transition sequences used in the present astrophysical identifications are listed in Table A.1. In labelling the sequences we conform, as closely as possible, to the notation of Koput (1986) in order to ensure traceability. There are only two differences where the original notation was ambiguous and was modified. In the case of the ground state, $v_b = 0$, $m = 0$, for which asymmetric rotor notation would normally be more appropriate, we modified Koput's notation to $K = 1$L, 1U, etc., to distinguish between lower and upper frequency sequences for the same value of K_a. Similarly, we used the notation $m = 3$L and 3U in order to distinguish between those of the two nearly degenerate $m = 3$ substates which give rise to lower and upper frequency rotational transition sequences.

The series fits and the Loomis-Wood displays were an invaluable aid to the analysis that allowed the identification of sequences of lines, extending up from the lowest J rotational transitions. It should be stated, however, that the transition frequencies for CH_3NCO reported in the line lists below are actual experimental frequencies. The power expansion fits were used to interpolate between the measured lines only in several cases of transitions missing in the spectrum for technical reasons. It is anticipated that these expansions may have useful predictive properties outside the present data region, but only for those series for which the expansion containing a moderate number of expansion terms is sufficient.

Appendix A.1: Spectroscopic constants and the partition function

The line lists for astrophysical detection require not only reliable line frequencies, but also line intensities that ultimately have a bearing on the derived column densities. Calculation of line intensities is crucially dependent on the rotational partition function, $Q_{\rm rot}$, and CH_3NCO also poses a considerable inconvenience in this respect. For asymmetric rotor molecules with vibrational modes at relatively high frequencies the ground vibrational state rotational partition function can be usefully approximated with

$$Q_{\rm rot} = 5.3311 \times 10^6 (T^3/(ABC))^{1/2}, \quad \text{(A.2)}$$

where A, B, and C are the rotational constants for the molecule (in MHz) and T is the temperature (in K). Assumption of the rotational partition function for just the ground state

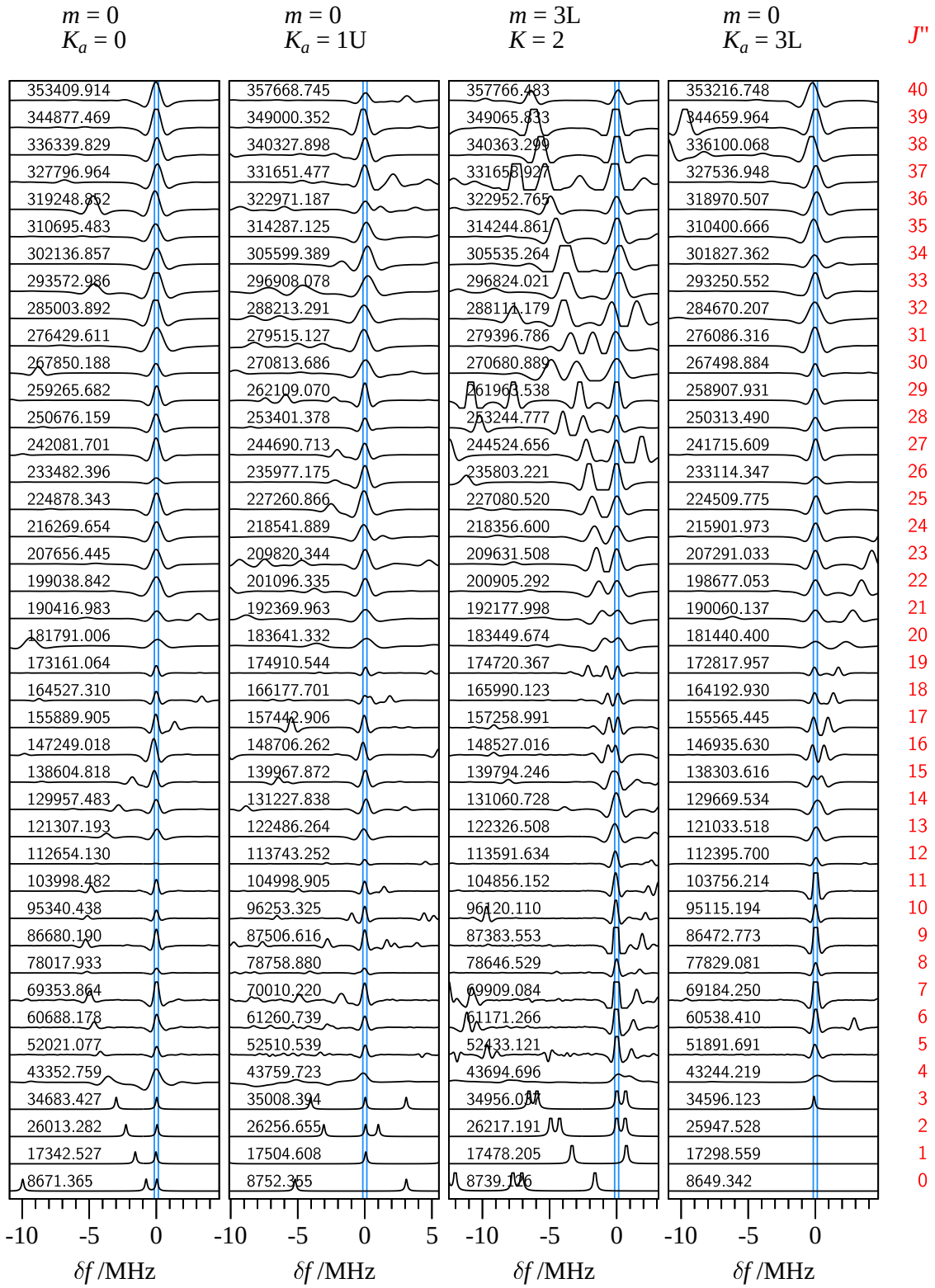

Fig. A.1. Sample Loomis-Wood type plots of the rotational spectrum of CH_3NCO for several assigned line sequences for $v_b = 0$ where sections of the experimental spectrum are plotted around the indicated centre frequencies from the linear-type fits. The plots illustrate how the assignments reached with Stark spectroscopy at $J'' \leq 3$ could be unambiguously transferred to the millimetre wave region. The blue lines mark the estimated frequency uncertainty.

Table A.1. The parameters of the linear rotor-type, $J(J+1)$ power series fitted to the assigned line sequences.

K^a	Name^b	I^c_{rel}	N^d_{in}	N^e_{rej}	s^f (MHz)	B^g (MHz)	D_J (kHz)	H_J (Hz)	L_J (mHz)	P_J (μHz)	P_{12} (nHz)	P_{14} (pHz)	P_{16} (fHz)	P_{18} (aHz)
v_b = 0, m = 0 (gs): E_{vib} = 0 cm^{-1}														
0	V093:	0.885	41	1	0.046	4335.6996 (13)	8.4815 (43)	0.1971 (58)	0.0728 (33)	-0.00909 (69)				
1L	V126:	0.842	38	2	0.048	4297.6203 (10)	3.3744 (21)	0.1133 (16)	-0.00393 (41)					
1U	V131:	0.819	38	2	0.062	4376.1857 (14)	4.2752 (30)	-0.0053 (24)	0.00245 (67)					
2L	V089:	0.833	38	1	0.055	4339.69609 (82)	3.28715 (94)	0.03891 (31)						
2U	V006:	0.901	38	1	0.052	4339.6811 (16)	-2.8764 (56)	-0.1690 (77)	-0.0676 (47)	0.0079 (10)				
3L	V096:	0.727	35	4	0.063	4324.6816 (20)	5.1755 (65)	-0.2787 (86)	0.1698 (50)	-0.0156 (10)				
3U	V097:	0.726	35	4	0.054	4324.6762 (18)	5.1686 (55)	-0.1769 (74)	0.1479 (43)	-0.01455 (89)				
v_b = 0, m = 1 E: E_{vib} = 8.4 cm^{-1}														
0a	V107:	0.808	22	0	0.051	4357.5774 (71)	132.34 (14)	86.4 (14)	226.1 (67)	-665. (17)	719. (21)	-298. (11)		
0b	X107:	0.808	20	0	0.056	4348.7 (10)	116.2 (37)	146.2 (74)	-125.4 (87)	71.4 (65)	-25.9 (29)	5.39 (74)	-0.493 (81)	
-1	V101:	0.836	39	1	0.050	4282.7615 (32)	-3.118 (26)	9.39 (10)	-10.67 (19)	6.64 (21)	-2.59 (13)	0.590 (44)	-0.0593 (59)	
1	V098:	0.846	36	5	0.048	4284.5720 (42)	-35.940 (44)	-45.38 (21)	49.98 (57)	-45.27 (87)	29.62 (81)	-12.71 (44)	3.16 (12)	-0.342 (15)
-2	not assigned													
2	V010:	0.660	31	2	0.042	4350.3415 (23)	-2.325 (15)	-0.065 (46)	-0.290 (64)	0.284 (43)	-0.109 (11)			
-3	V005:	0.800	36	2	0.058	4343.3487 (25)	0.096 (11)	0.288 (25)	-0.381 (25)	0.202 (12)	-0.0848 (22)			
3	V012:	0.642	34	3	0.049	4356.1489 (11)	1.6845 (24)	-0.0204 (19)	0.00189 (52)					
v_b = 0, m = −2 E: E_{vib} = 36.8 cm^{-1}														
0	V119:	0.774	36	1	0.050	4356.2099 (29)	2.431 (15)	0.837 (33)	-2.676 (29)					
-1	V008:	0.708	38	2	0.062	4353.2529 (11)	1.0831 (14)	0.0	0.00928 (84)	-0.00378 (31)				
1	V180:	0.807	40	0	0.188	4350.771 (14)	-40.79 (16)	-39.36 (81)	-24.5 (22)	74.5 (34)	-69.5 (32)	34.7 (17)	-9.27 (54)	1.045 (69)
-2	not assigned													
2	V100:	0.805	39	0	0.084	4276.5950 (66)	-51.195 (68)	-64.24 (33)	63.79 (84)	-50.5 (12)	29.3 (11)	-11.35 (59)	2.60 (17)	-0.262 (20)
-3	V024:	0.473	35	3	0.055	4366.9265 (12)	1.9129 (27)	-0.0098 (22)	0.00672 (61)					
3a	V106:	0.523	21	0	0.043	4373.6038 (50)	110.306 (69)	93.71 (41)	-32.2 (12)	-11.7 (16)	10.81 (88)			
3b	X106:	0.884	18	0	0.052	4370.20 (59)	103.8 (16)	95.6 (24)	-55.9 (22)	20.9 (11)	-4.49 (32)	0.438 (38)		
v_b = 0, m = 3L (K = 0, J = 0, 1 = A_1, A_2): E_{vib} = 80.3 cm^{-1}														
0	V017:	0.556	38	2	0.061	4361.0342 (19)	0.6664 (66)	0.0255 (94)	0.0843 (57)	-0.0269 (12)				
-1	V137:	0.654	37	2	0.093	4376.0833 (78)	-11.011 (83)	3.34 (41)	-25.5 (11)	21.8 (17)	-17.3 (16)	11.56 (91)	-4.15 (27)	0.576 (34)
1	V082:	0.485	39	0	0.070	4362.15134 (58)	1.68176 (26)							
-2	not assigned													
2	V030:	0.399	35	3	0.067	4369.5669 (10)	1.9458 (12)	-0.00228 (41)						
3	V040:	0.634	33	2	0.064	4378.65685 (60)	2.06406 (30)							
v_b = 0, m = 3U (K = 0, J = 1, 0 = A_2, A_1): E_{vib} = 79.7 cm^{-1}														
0	V018:	0.540	39	2	0.046	4361.4499 (14)	0.5247 (49)	0.0221 (69)	0.0949 (42)	-0.02898 (93)				
1	V020:	0.491	36	3	0.044	4363.55034 (68)	1.72074 (80)	-0.00110 (27)						
-1	not assigned													
2	V029:	0.424	34	4	0.057	4369.57115 (94)	1.9779 (10)	0.00072 (36)						
-2	not assigned													
3	very strongly perturbed													
v_b = 0, m = 4 E: E_{vib} = 140.6 cm^{-1}														
0	V025:	0.416	37	3	0.052	4368.7341 (11)	1.5662 (25)	0.0039 (21)	0.00218 (57)					
v_b = 0, m = −5 E: E_{vib} = 217.5 cm^{-1}														
0	V142:	0.297	38	1	0.049	4377.7029 (11)	1.8930 (23)	-0.0136 (19)	0.00256 (51)					
v_b = 1, m = 0 : E_{vib} = 182.2 cm^{-1}														
0	V094:	0.391	41	0	0.050	4335.3010 (15)	7.8017 (47)	0.2011 (63)	0.0443 (37)	-0.00561 (76)				
1L	V127:	0.373	38	2	0.052	4297.1113 (11)	3.2544 (22)	0.0971 (17)	-0.00294 (44)					
1U	V132:	0.365	36	3	0.048	4377.6225 (11)	4.2356 (24)	0.0116 (19)	0.00223 (53)					

Notes.

[a] The value of the K_a or K quantum number following, where possible, the notation of Koput (1986) and described further in the text following Eq.A.1.

[b] The identifier of the line sequence, identifiers Vnnn and Xnnn for the same "nnn" denote a two part sequence (Vnnn lower, Xnnn higher frequency part).

[c] Intensity of the sequence relative to the strongest sequence in the spectrum.

[d] The number of lines in the linear fit.

[e] The number of confidently assigned lines that were perturbed and were rejected from the fit.

[f] The standard deviation od the linear fit.

[g] The values of the parameters required in the linear fit.

of the molecule as the total partition function and neglect of population in excited vibrational states is normally associated with a relatively small underestimate, especially for low-temperature environments. For CH_3NCO this is not the case owing to the plethora of low-lying internal rotation substates, and it is necessary to consider the vibration-rotation partition function, Q_{vr}, explicitly. Furthermore, the difficulties in fitting more than a relatively small subset of measured transitions affect even the determination of the rotational constants. We summarize the situation in Table A.2, which demonstrates that even with a consider-

able reduction in the range of K_a values for the fitted transitions, the fit is less satisfactory than is usually the case with rotational spectra. Inclusion of measured transitions for all measured values of J requires the use of a rather large number of centrifugal distortion constants and values of some of these constants are also of considerable magnitude. This points to the very effective nature of such constants and to the considerable vibration-rotation interactions in the CH_3NCO molecule. The deviation of fit is also somewhat greater than the experimental accuracy. With these reservations in mind, we find rather good agreement between rotational constants resulting from the two fits based on very different subsets of the current data (the two central columns of Table A.2). We therefore use the combined fit of the indicated limited data (the rightmost column of Table A.2) as the source of rotational constants for evaluation of the partition function. The complete results of that fit are reported in Table A.3.

The second issue affecting the evaluation of the partition function is the summation over the energy levels. We used the SPCAT program to carry out this summation numerically, and the results are summarized in Table A.4. The nearly free internal rotor levels $m = 1, 2, 4, 5$ are closer in character to the symmetric top case so that we used rotational constants A and $(B + C)/2$ in the partition function calculation, while for the remaining sublevels ($m = 0$ and m being a multiple of 3) we used separate values of A, B, and C (all from the final column of Table A.2). It can be seen in Table A.4 (a) that at room-temperature and at a specimen astrophysical temperature of 120 K the partition function Q_{vr} increases significantly on addition of successive vibrational substates. It is only upon reaching vibrational energy of 400 cm^{-1} above the ground state that a moderate saturation of the value of Q_{vr} becomes apparent. This corresponds to the consideration of energy levels in the ground state and the 17 vibrational substates immediately above it.

Table A.4(b) further illustrates some technical aspects associated with the evaluation of Q_{vr} such as the necessity of using sufficiently broad limits on the values of the J and K quantum numbers. It turns out that the large values of centrifugal distortion constants from the effective fit for $K \leq 2$ lead to unphysical compression of energy levels at the highest values of J and K, as highlighted by specific diagnostics from the SPCAT program. At the same time, the details of the summation have little effect on the estimate of the low temperature partition function. For this reason we settle on the "recommended" conditions, which pass the test that the value from the numerical summation for just the ground state is close to that from the analytical formula in Eq. A.2.

The final result of these considerations is that at room-temperature it is necessary to use a partition function value that is almost 8 times greater than that for just the ground state, while at 120 K this ratio is closer to 4. It is clear that a reliable estimate of the partition function to use for the calculation of transition intensities will have a direct bearing on the derived astrophysical abundances of CH_3NCO.

Appendix A.2: Line lists

The final results of the analysis of the laboratory rotational spectrum of CH_3NCO for use in astrophysical applications are presented in Tables A.5 and A.6. The experimental frequencies for 27 rotational transition sequences with the lowest vibrational energy are listed in Table A.5. Five more specimen transition sequences corresponding to higher vibrational energies and presenting a challenge to confident astrophysical detection are also included. This line list is also given in Table A.6 in the standard format of the JPL catalog (Pickett et al. 1998). Table A.6 contains line intensities and lower state energies so that it can be easily converted to a different temperature. Table A.6 constitutes the main tool for astrophysical detection and characterization of CH_3CNO, and we summarize the key parameters used in its evaluation: $\mu = \mu_a = 2.882$ D, $T = 300$ K, and $Q_{vr} = 138369$ calculated by summing over rotational levels limited by $K < 11$ and $J < 100$ for all vibrational states up to 402.5 cm^{-1} above the ground state.

We have already commented above on the key discrepancies between the experimental frequencies reported in Halfen et al. (2015) and those in this work as summarized in Table A.7. We further note that if we replace our frequencies in the fit for the ground state reported in Table A.3 by the three problematic $m = 0$ lines at 60160.932, 68753.890, and 70009.179 MHz (see Table A.7), then those lines are incompatible with this fit at obs.-calc. frequencies of near -1.1 MHz. Our frequencies for these transitions have obs.-calc. values of less than 0.03 MHz, in a fit encompassing 201 pure rotational transition frequencies. In fact, the discrepancy of 1 MHz from a line sequence comprising around 40 lines and consisting of both Koput (1986) and our mm-wave lines would be immediately visible. This is clearly apparent in Fig. A.1 (second column from the left), where the 70010.208 MHz line is in good agreement with the sequence defined by a low order $J(J + 1)$-type fit, whereas a frequency of 70009.179 MHz is clearly incompatible.

Finally, we note that the quantization used in Halfen et al. (2015) for the $m = 0$, $K_a = 1$ transitions deviates from standard practice. While the quantization for the $m > 0$ lines is somewhat arbitrary and largely dependent on the fitting program, the quantization for the ground state is well established. In the case when the splitting between the two a-dipole $\Delta J = 1$, $K_a = 1$ transitions for a given value of J'' is dominated by the asymmetry term in the rotational Hamiltonian (as is the case for CH_3NCO) it is the $K_a = 1$ transition with the *higher* value of K_c that is at *lower* frequency, and the one with *lower* value of K_c that is at *higher* frequency. This quantization leads to the moderately successful effective fit for the ground ($m = 0$) state reported by us in Table A.3. On the other hand, in Halfen et al. (2015) the K_c quantization for m=0, K_a=1 transitions is systematically reversed.

Appendix A.3: Nuclear quadrupole hyperfine splitting

It should be noted that the lowest-J rotational transitions of CH_3NCO are subject to nuclear quadrupole hyperfine splitting, and that the line lists discussed above provide in such cases only the average, hyperfine-free frequencies. The hyperfine splitting arising from the presence of the ^{14}N nucleus in the CH_3NCO molecule was studied in previous works (Kasten & Dreizler 1986; Curl et al. 1963; Lett et al. 1967). We have now, for the first time, observed such lines at the very low temperature of supersonic expansion using two spectroscopic techniques. CH_3NCO was first investigated by broadband chirped-pulse Fourier transform microwave (CP-FTMW) spectroscopy (Brown et al. 2008) in two different frequency ranges: 6 – 18 and 25 – 26 GHz (Mata et al. 2012). A gas mixture containing 0.3% of CH_3NCO in neon at the backing pressure of 3 bar was used for the pulsed jet expansion. These scans allowed explicit confirmation of the assignment of the ground state ($v_b = 0$, $m = 0$) lines since these lines (and some of the lowest $v_b = 0$, $m = 1$ substate lines) are the only lines expected to be visible at these conditions. In order to resolve the nuclear quadrupole hyperfine

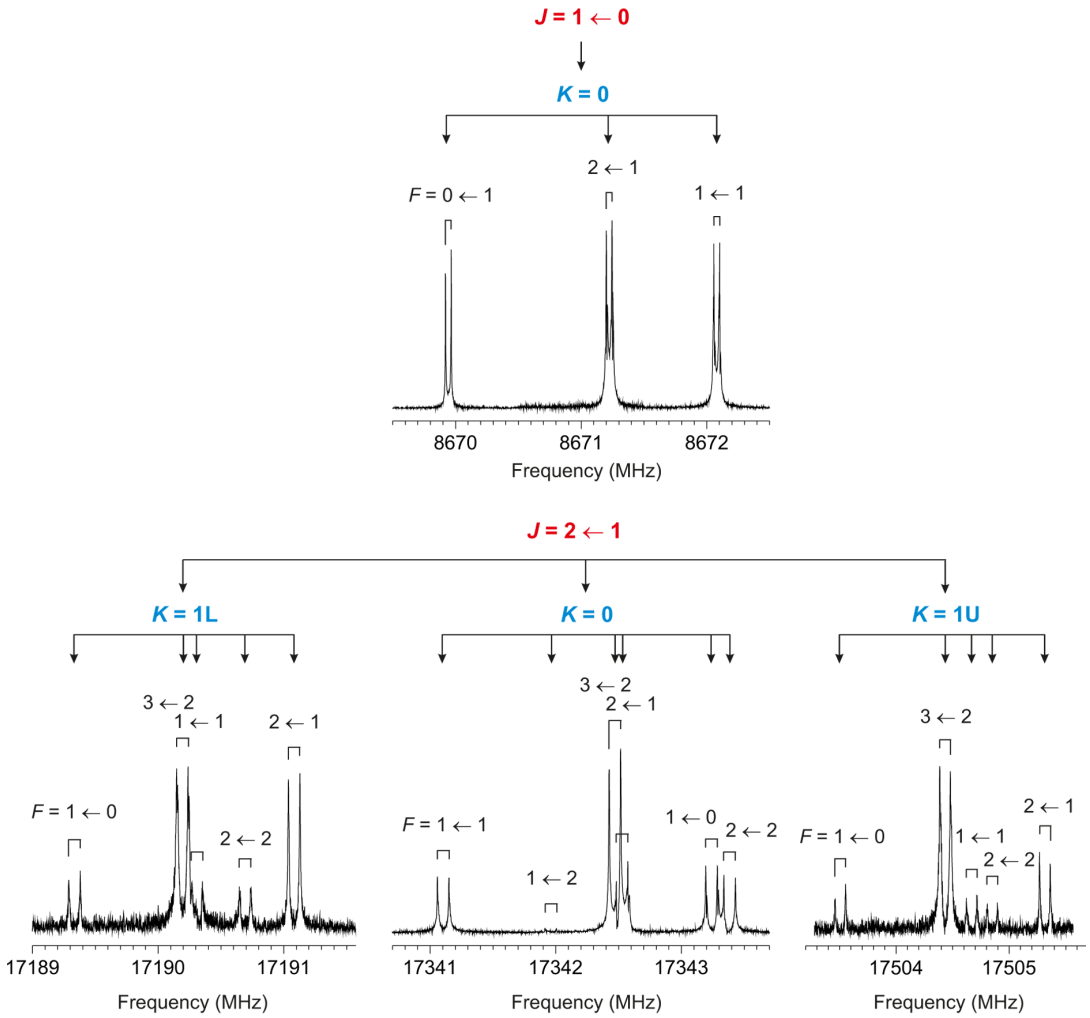

Fig. A.2. Splitting patterns in the lowest-J rotational transitions in the ground state ($v_b = 0$, $m = 0$) of CH_3NCO. The splitting is due to the interaction of the nuclear quadrupole of the ^{14}N nucleus with molecular rotation and is characterized by the total angular momentum quantum number F. Each component is doubled by the Doppler doubling, which is an instrumental effect specific to the FP-FTMW spectrometer. The splitting is completely resolved at the supersonic expansion conditions ($T_{rot} = 2$ K) of the FP-FTMW spectrometer. Nevertheless, the magnitude, and thus the relevance of the splitting, decreases rapidly with increasing J.

structure, further measurements were performed by supersonic expansion, Fabry-Perot cavity, and Fourier transform microwave (FP-FTMW) spectroscopy (Grabow et al. 1996) using two different configurations covering the frequency range from 4 to 18 GHz (Alonso et al. 1997; Bermúdez et al. 2014). Fig. A.2 shows the experimentally recorded hyperfine patterns for the first two lowest-J transitions of CH_3NCO and it is clear that at sub-MHz resolution consideration of such splitting is important. Table A.8 lists hyperfine component frequencies for all $K \leq 2$ rotational transitions up to 80 GHz. This prediction has an estimated accuracy of around 5 kHz and was made by using the rightmost set of spectroscopic constants from Table A.2. It is apparent that the central $\Delta F = +1$ components quickly coalesce, while the outer $\Delta F = 0$ components rapidly lose intensity.

Table A.2. Spectroscopic constants determined for the ground state of CH_3NCO ($v_b = 0$, $m = 0$).

Constant	Koput (1986)	Hyperfine resolved $J \leq 2, K_a \leq 1$	Hyperfine unresolved $J \leq 42, K_a \leq 2$	All data
A^a (MHz)	73849.2	128356.(7623)[b]	128435.(19)	128402.(13)
B (MHz)	4392.22	4414.2478(12)	4414.6182(93)	4414.6287(75)
C (MHz)	4256.66	4257.1309(12)	4256.7490(85)	4256.7452(71)
Δ_J (kHz)		2.45(40)	2.3209(11)	2.32319(98)
Δ_{JK} (kHz)		−1202.3(23)	−1274.0(13)	−1271.46(73)
δ_J (kHz)			0.4042(14)	0.4038(14)
δ_K (kHz)			183.1(43)	187.4(35)
Φ_J (Hz)			−0.00191(47)	−0.00142(45)
Φ_{JK} (Hz)			−5.39(24)	−5.64(18)
Φ_{KJ} (Hz)			−68478.(285)	−67991.(167)
ϕ_{JK} (Hz)			−47.6(14)	−47.7(14)
χ_{aa} (MHz)	2.8358(75)	2.8461(18)		2.8441(49)
χ_{bb} (MHz)	−1.288(21)	−1.2981(30)		−1.2962(67)
χ_{cc} (MHz)	−1.548(21)	−1.5481(30)		−1.5478(67)
$N^c_{\rm lines}$	13	32	201	233
$\sigma^d_{\rm fit}$ (kHz)	6	3	94.6	91.2
$\sigma^e_{\rm rms}$	0.842	0.674	1.89	1.87

Notes.
[(a)] A, B, and C are rotational constants; $\Delta_J, ..., \phi_{JK}$ are centrifugal distortion constants in Watson's A-reduced asymmetric rotor Hamiltonian; and $\chi_{aa}, \chi_{bb}, \chi_{cc}$ are nuclear quadrupole hyperfine splitting constants for the ^{14}N nucleus.
[(b)] Errors in parentheses are standard errors in units of the last digit.
[(c)] The number of fitted lines.
[(d)] Standard deviation of the fit.
[(e)] Unitless (weighted) deviation of the fit.

Table A.3. Results of fitting the spectroscopic constants of Table A.2 for CH_3NCO ground state (m=0).

J'	Ka'	Kc'	F'	J"	Ka"	Kc"	F"	obs. (MHz)	o.-c. (MHz)	error (MHz)
Valladolid supersonic expansion, cavity FTMW										
(small splitting in some components averaged)										
1	0	1	0	0	0	0	1	8669.9439	0.0013	0.003
1	0	1	2	0	0	0	1	8671.2271	0.0047	0.005
1	0	1	1	0	0	0	1	8672.0809	0.0053	0.005
2	0	2	1	1	0	1	1	17341.1048	0.0012	0.003
2	0	2	1	1	0	1	2	17341.9591	0.0023	0.003
2	0	2	3	1	0	1	2	17342.4705	0.0059	0.003
2	0	2	2	1	0	1	1	17342.5315	0.0059	0.005
2	0	2	1	1	0	1	0	17343.2442	0.0076	0.005
2	0	2	2	1	0	1	2	17343.3848	0.0059	0.003
2	1	2	1	1	1	1	0	17189.3349	0.0021	0.003
2	1	2	3	1	1	1	2	17190.1971	0.0046	0.005
2	1	2	1	1	1	1	1	17190.3077	0.0027	0.003
2	1	2	2	1	1	1	2	17190.6905	0.0005	0.003
2	1	2	2	1	1	1	1	17191.0845	0.0056	0.003
2	1	1	1	1	1	0	0	17503.5055	-0.0029	0.003
2	1	1	3	1	1	0	2	17504.4327	-0.0037	0.003
2	1	1	1	1	1	0	1	17504.6671	-0.0022	0.003
2	1	1	2	1	1	0	2	17504.8506	-0.0025	0.003
2	1	1	2	1	1	0	1	17505.3161	-0.0013	0.003
Kasten + Dreizler										
1	0	1	0	0	0	0	1	8669.9540	0.0114	0.005
1	0	1	2	0	0	0	1	8671.2240	0.0016	0.005
1	0	1	1	0	0	0	1	8672.0790	0.0033	0.005
2	0	2	3	1	0	1	2	17342.4670	0.0023	0.005
2	0	2	2	1	0	1	1	17342.5360	0.0104	0.005
2	0	2	1	1	0	1	0	17343.2340	-0.0025	0.005
2	0	2	2	1	0	1	2	17343.3790	0.0001	0.005
2	1	2	1	1	1	1	0	17189.3380	0.0052	0.005
2	1	2	3	1	1	1	2	17190.1970	0.0046	0.005
2	1	2	2	1	1	1	1	17191.0820	0.0031	0.005
2	1	1	1	1	1	0	0	17503.5090	0.0005	0.005
2	1	1	3	1	1	0	2	17504.4390	0.0026	0.005
2	1	1	2	1	1	0	1	17505.3220	0.0045	0.005
Hyperfine-free lines: Koput + MMW Valladolid + FASSST										
1	0	1		0	0	0		8671.4100	0.0454	0.050
2	0	2		1	0	1		17342.5000	-0.0255	0.050
3	0	3		2	0	2		26013.3400	0.0604	0.050
4	0	4		3	0	3		34683.4600	0.0365	0.050
5	0	5		4	0	4		43352.7630	0.0083	0.050
6	0	6		5	0	5		52021.1060	0.0350	0.050
7	0	7		6	0	6		60688.2100	0.0387	0.050
8	0	8		7	0	7		69353.8800	0.0247	0.050
9	0	9		8	0	8		78017.9530	0.0292	0.050
10	0	10		9	0	9		86680.1900	0.0106	0.050
11	0	11		10	0	10		95340.4430	0.0172	0.050
12	0	12		11	0	11		103998.4810	0.0120	0.050
13	0	13		12	0	12		112654.0590	-0.0580	0.050
14	0	14		13	0	13		121307.2370	0.0565	0.050
15	0	15		14	0	14		129957.4710	-0.0016	0.050
16	0	16		15	0	15		138604.6700	-0.1401	0.050
17	0	17		16	0	16		147248.8260	-0.1869	0.050
18	0	18		17	0	17		155889.8670	-0.0382	0.050
19	0	19		18	0	18		164527.3080	-0.0074	0.050
20	0	20		19	0	19		173161.0610	-0.0158	0.050
21	0	21		20	0	20		181791.1040	0.0759	0.050
22	0	22		21	0	21		190417.0240	0.0104	0.050
23	0	23		22	0	22		199038.8460	-0.0381	0.050
24	0	24		23	0	23		207656.4340	-0.0633	0.050
25	0	25		24	0	24		216269.6740	-0.0442	0.050
26	0	26		25	0	25		224878.3540	-0.0656	0.050
27	0	27		26	0	26		233482.3920	-0.0910	0.050
28	0	28		27	0	27		242081.6800	-0.1184	0.050
29	0	29		28	0	28		250676.1400	-0.1257	0.050
30	0	30		29	0	29		259265.7080	-0.0864	0.050
31	0	31		30	0	30		267850.1630	-0.1414	0.050
32	0	32		31	0	31		276429.6520	-0.0742	0.050
33	0	33		32	0	32		285003.8410	-0.1606	0.050
34	0	34		33	0	33		293572.9900	-0.0933	0.050
35	0	35		34	0	34		302136.8980	-0.0380	0.050
36	0	36		35	0	35		310695.4270	-0.1085	0.050
37	0	37		36	0	36		319248.7530	-0.1168	0.050
38	0	38		37	0	37		327797.0500	0.1116	0.050
39	0	39		38	0	38		336339.8860	0.1341	0.050
40	0	40		39	0	39		344877.4680	0.1351	0.050
41	0	41		40	0	40		353409.8830	0.1685	0.050
42	0	42		41	0	41		361937.2030	0.2623	0.050
2	1	2		1	1	1		17190.6700	0.3022	0.050
3	1	3		2	1	2		25785.4100	0.0606	0.050
4	1	4		3	1	3		34380.1400	0.0516	0.050
5	1	5		4	1	4		42974.4300	-0.0743	0.050
6	1	6		5	1	5		51568.5290	0.0117	0.050
7	1	7		6	1	6		60162.0760	0.0288	0.050
8	1	8		7	1	7		68755.0250	0.0099	0.050
9	1	9		8	1	8		77347.4250	0.0828	0.050
10	1	10		9	1	9		85938.9620	0.0115	0.050
11	1	11		10	1	10		94529.7610	-0.0016	0.050
12	1	12		11	1	11		103119.7030	0.0008	0.050
13	1	13		12	1	12		111708.7070	0.0135	0.050
14	1	14		13	1	13		120296.6300	-0.0318	0.050
15	1	15		14	1	14		128883.6440	0.1105	0.050
16	1	16		15	1	15		137469.2870	0.0511	0.050
17	1	17		16	1	16		146053.5740	-0.1234	0.050
18	1	18		17	1	17		154636.8670	0.0190	0.050
19	1	19		18	1	18		163218.6020	-0.0162	0.050
20	1	20		19	1	19		171798.9900	0.0492	0.050
21	1	21		20	1	20		180377.7680	0.0191	0.050
22	1	22		21	1	21		188955.1000	0.1222	0.050
23	1	23		22	1	22		197530.5550	-0.0088	0.050
24	1	24		23	1	23		206104.4470	0.0019	0.050
25	1	25		24	1	24		214676.5300	-0.0308	0.050
26	1	26		25	1	25		223246.8260	-0.0262	0.050
27	1	27		26	1	26		231815.2500	-0.0118	0.050
28	1	28		27	1	27		240381.6640	-0.0699	0.050
29	1	29		28	1	28		248946.1500	-0.0642	0.050
30	1	30		29	1	29		257508.6010	-0.0494	0.050
31	1	31		30	1	30		266068.9260	-0.0654	0.050
32	1	32		31	1	31		274627.1410	-0.0472	0.050
33	1	33		32	1	32		283183.2160	0.0227	0.050
34	1	34		33	1	33		291736.8910	-0.0696	0.050
35	1	35		34	1	34		300288.3190	-0.1272	0.050
36	1	36		35	1	35		308837.5260	-0.0814	0.050
37	1	37		36	1	36		317384.4490	0.0455	0.050
38	1	38		37	1	37		325928.8020	0.0070	0.050
39	1	39		38	1	38		334470.6160	-0.1282	0.050

J'	Ka'	Kc'	F'	J"	Ka"	Kc"	F"	obs. (MHz)	o.-c. (MHz)	error (MHz)
40	1	40		39	1	39		343010.1490	-0.0662	0.050
41	1	41		40	1	40		351547.2590	0.0855	0.050
42	1	42		41	1	41		360081.6650	0.0791	0.050
2	1	1		1	1	0		17504.6800	0.0736	0.050
3	1	2		2	1	1		26256.7100	0.0570	0.050
4	1	3		3	1	2		35008.4300	0.0383	0.050
5	1	4		4	1	3		43759.6000	-0.1197	0.050
6	1	5		5	1	4		52510.5630	0.0283	0.050
7	1	6		6	1	5		61260.7340	0.0003	0.050
8	1	7		7	1	6		70010.2080	-0.0061	0.050
9	1	8		8	1	7		78758.8490	-0.0242	0.050
10	1	9		9	1	8		87506.6070	-0.0014	0.050
11	1	10		10	1	9		96253.3180	0.0010	0.050
12	1	11		11	1	10		104998.8860	-0.0099	0.050
13	1	12		12	1	11		113743.2410	-0.0017	0.050
14	1	13		13	1	12		122486.1730	-0.0815	0.050
15	1	14		14	1	13		131227.9270	0.0983	0.050
16	1	15		15	1	14		139967.9030	0.0408	0.050
17	1	16		16	1	15		148706.1240	-0.1284	0.050
18	1	17		17	1	16		157442.8620	-0.0346	0.050
19	1	18		18	1	17		166177.7250	0.0329	0.050
20	1	19		19	1	18		174910.5960	0.0600	0.050
21	1	20		20	1	19		183641.4610	0.1354	0.050
22	1	21		21	1	20		192370.0130	0.0546	0.050
23	1	22		22	1	21		201096.3660	0.0342	0.050
24	1	23		23	1	22		209820.3630	0.0198	0.050
25	1	24		24	1	23		218541.8030	-0.0873	0.050
26	1	25		25	1	24		227260.7990	-0.0719	0.050
27	1	26		26	1	25		235977.1810	-0.0017	0.050
28	1	27		27	1	26		244690.7010	-0.0229	0.050
29	1	28		28	1	27		253401.3880	-0.0047	0.050
30	1	29		29	1	28		262109.0720	-0.0154	0.050
31	1	30		30	1	29		270813.7400	0.0330	0.050
32	1	31		31	1	30		279515.0450	-0.1052	0.050
33	1	32		32	1	31		288213.2250	-0.0916	0.050
34	1	33		33	1	32		296908.3040	0.1980	0.050
35	1	34		34	1	33		305599.5880	0.1696	0.050
36	1	35		35	1	34		314287.2370	0.0824	0.050
37	1	36		36	1	35		322971.2260	0.0103	0.050
38	1	37		37	1	36		331651.4570	-0.0465	0.050
39	1	38		38	1	37		340327.9230	0.0023	0.050
40	1	39		39	1	38		349000.2270	-0.1433	0.050
41	1	40		40	1	39		357668.8020	0.0454	0.050
3	2	2		2	2	1		26038.2000	0.3438	0.050
4	2	3		3	2	2		34716.9100	0.1374	0.050
5	2	4		4	2	3		43395.5400	0.1671	0.050
6	2	5		5	2	4		52073.4700	-0.1083	0.050
7	2	6		6	2	5		60751.2420	-0.0683	0.050
8	2	7		7	2	6		69428.4030	-0.0873	0.050
9	2	8		8	2	7		78104.9430	-0.0972	0.050
10	2	9		9	2	8		86780.7780	-0.1038	0.050
11	2	10		10	2	9		95455.8140	-0.1235	0.050
12	2	11		11	2	10		104130.0100	-0.1199	0.050
13	2	12		12	2	11		112803.2580	-0.1239	0.050
14	2	13		13	2	12		121475.4960	-0.1208	0.050
15	2	14		14	2	13		130146.7990	0.0408	0.050
16	2	15		15	2	14		138816.7390	0.0087	0.050
17	2	16		16	2	15		147485.3600	-0.0974	0.050
18	2	17		17	2	16		156152.7430	-0.1219	0.050
19	2	18		18	2	17		164818.8450	-0.0332	0.050
20	2	19		19	2	18		173483.4660	0.0426	0.050
21	2	20		20	2	19		182146.4730	0.0458	0.050
22	2	21		21	2	20		190807.8310	0.0143	0.050
23	2	22		22	2	21		199467.5590	0.0390	0.050
24	2	23		23	2	22		208125.4910	0.0254	0.050
25	2	24		24	2	23		216781.6210	0.0382	0.050
26	2	25		25	2	24		225435.8490	0.0476	0.050
27	2	26		26	2	25		234088.1250	0.0727	0.050
28	2	27		27	2	26		242738.3090	0.0422	0.050
29	2	28		28	2	27		251386.4480	0.0707	0.050
30	2	29		29	2	28		260032.3910	0.0742	0.050
31	2	30		30	2	29		268676.1360	0.1167	0.050
32	2	31		31	2	30		277317.4920	0.0724	0.050
33	2	32		32	2	31		285956.5910	0.1375	0.050
34	2	33		33	2	32		294593.2450	0.1876	0.050
35	2	34		34	2	33		303227.2980	0.1288	0.050
36	2	35		35	2	34		311858.7810	0.0538	0.050
37	2	36		36	2	35		320487.6960	0.0250	0.050
38	2	37		37	2	36		329113.8250	-0.1161	0.050
39	2	38		38	2	37		337737.4330	-0.0463	0.050
40	2	39		39	2	38		346358.1370	-0.0911	0.050
41	2	40		40	2	39		354975.8680	-0.2633	0.050
3	2	1		2	2	0		26038.2000	-0.2472	0.050
4	2	2		3	2	1		34718.1100	-0.1397	0.050
5	2	3		4	2	2		43398.2650	-0.0609	0.050
6	2	4		5	2	3		52078.6310	-0.1122	0.050
7	2	5		6	2	4		60759.4890	-0.0795	0.050
8	2	6		7	2	5		69440.7720	-0.0958	0.050
9	2	7		8	2	6		78122.5870	-0.1191	0.050
10	2	8		9	2	7		86805.0270	-0.1203	0.050
11	2	9		10	2	8		95488.1310	-0.1230	0.050
12	2	10		11	2	9		104171.9620	-0.1249	0.050
13	2	11		12	2	10		112856.5850	-0.1202	0.050
14	2	12		13	2	11		121542.1130	-0.0526	0.050
15	2	13		14	2	12		130228.4190	-0.1035	0.050
16	2	14		15	2	13		138915.6030	-0.2246	0.050
17	2	15		16	2	14		147603.9630	-0.1665	0.050
18	2	16		17	2	15		156293.3170	-0.1560	0.050
19	2	17		18	2	16		164983.8810	-0.0181	0.050
20	2	18		19	2	17		173675.3920	-0.0527	0.050
21	2	19		20	2	18		182368.2180	0.0764	0.050
22	2	20		21	2	19		191062.0290	0.0127	0.050
23	2	21		22	2	20		199757.0680	-0.0215	0.050
24	2	22		23	2	21		208453.3650	-0.0110	0.050
25	2	23		24	2	22		217150.9320	0.0484	0.050
26	2	24		25	2	23		225849.6710	0.0584	0.050
27	2	25		26	2	24		234549.6360	0.0803	0.050
28	2	26		27	2	25		243250.7340	0.0367	0.050
29	2	27		28	2	26		251953.1080	0.0948	0.050
30	2	28		29	2	27		260656.5870	0.1172	0.050
31	2	29		30	2	28		269361.1960	0.1722	0.050
32	2	30		31	2	29		278066.7380	0.1158	0.050
33	2	31		32	2	30		286773.1780	-0.0233	0.050
34	2	32		33	2	31		295480.8970	0.2095	0.050
35	2	33		34	2	32		304189.1200	0.1243	0.050
36	2	34		35	2	33		312898.1990	0.1688	0.050
37	2	35		36	2	34		321607.6950	0.0104	0.050
38	2	36		37	2	35		330317.8260	-0.0153	0.050
39	2	37		38	2	36		339028.2350	-0.1373	0.050
40	2	38		39	2	37		347738.9940	-0.1447	0.050
41	2	39		40	2	38		356449.7320	-0.2598	0.050

Table A.4. Determination of the partition function for transition intensity calculations.

(a) Evolution of the value of Q_{vr} on addition of successive vibrational states to the summation

$J_{lim} = 50$, $K_{lim} = 15$		E_{vib} (cm^{-1})	Q_{vr} (300 K)	Q_{vr} (120 K)
	$v_b = 0$ $m = 0$	0.0	15055	4474
+	$m = 1$	8.4	29292	8509
+	$m = 2$	36.8	41716	11379
+	$m = 3L$	80.3	51802	13083
+	$m = 3U$	79.7	61916	14799
+	$m = 4$	140.6	69468	15626
+	$m = 5$	217.5	74691	15955
+	$m = 6a$	311.1	78025	16062
+	$m = 6b$	311.1	81359	16169
+	$v_b = 1$ $m = 0$	182.2	87546	16671
	$m = 1$	191.4	93465	17121
	$m = 2$	222.3	98569	17431
	$m = 3a$	268.3	102663	17610
	$m = 3b$	268.9	106745	17788
	$m = 4$	333.4	109741	17870
+	$v_b = 2$ $m = 0$	357.9	112405	17931
	$m = 1$	368.6	114935	17984
	$m = 2$	402.5	117404	18035

(b) Sensitivity of the value of Q_{vr} to quantum number limits used in the numerical summation

	J_{lim}	K_{lim}	Q_{vr} (300 K)	Q_{vr} (120 K)
all[a]	50	10	113660	18021
all	70	10	132301	18223
all	100	10	136409	18225
all	50	15	117404	18035
all	70	15	136815	18237
all	100	15[b]	141159	18240
Recommended:				
	100	11		
all			138369	18235
only $v_b, m = 0, 0$			17744	4524
only $v_b, m = 0, 0$	analytical		17831	4511

Notes.
[a]Summation over all vibrational states up to 402.5 cm^{-1} ($v_b = 2$, $m = 2$). [b]Energy level compression problems at highest K and J due to large values of some centrifugal distortion constants in the effective fit.

Table A.5. Line list of rotational transitions for CH_3NCO compiled form experimental frequencies (MHz) for line sequences assigned on the basis of continuity from the assignment reached for $J''\leq 3$.

(a) v_b=0, m=0 (ground state), $E_{\rm vib}$ = 0 cm^{-1}

K^a =		0	1L	1U	2L	2U	3L	3U
J'	J''							
1	0	8671.410[b]						
2	1	17342.500	17190.670	17504.680				
3	2	26013.340	25785.410	26256.710	26038.200	26038.200		
4	3	34683.460	34380.140	35008.430	34716.910	34718.110	34596.030	34596.030
5	4	43352.763	42974.430	43759.600	43395.540	43398.265	43244.392	43244.392
6	5	52021.106	51568.529	52510.563	52073.470	52078.631	51891.662	51891.662
7	6	60688.210	60162.076	61260.734	60751.242	60759.489	60538.443	60538.443
8	7	69353.880	68755.025	70010.208	69428.403	69440.772	69184.277	69184.277
9	8	78017.953	77347.425	78758.849	78104..943	78122.587	77829.107	77829.107
10	9	86680.190	85938.962	87506.607	86780.778	86805.027	86472.805	86472.805
11	10	95340.443	94529.761	96253.318	95455.814	95488.131	95115.214	95115.214
12	11	103998.481	103119.703	104998.886	104130.010	104171.962	103756.254	103756.254
13	12	112654.059	111708.707	113743.241	112803.258	112856.585	112395.756	112395.756
14	13	121307.237	120296.630	122486.173	121475.496	121542.113	121033.586	121033.586
15	14	129957.471	128883.644	131227.927	130146.799	130228.419	129669.703	129669.703
16	15	138604.670	137469.287	139967.903	138816.739	138915.603	138303.496	138304.065
17	16	147248.826	146053.574	148706.124	147485.360	147603.963	146935.424	146936.284
18	17	155889.867	154636.867	157442.862	156152.743	156293.317	155565.312	155566.394
19	18	164527.308	163218.602	166177.725	164818.845	164983.881	164192.884	164194.278
20	19	173161.061	171798.990	174910.596	173483.466	173675.392	172817.892	172819.679
21	20	181791.104	180377.768[c]	183641.461	182146.473	182368.218	181440.422	181442.696
22	21	190417.024	188955.100	192370.013	190807.831	191062.029	190060.149	190062.937
23	22	199038.846	197530.555	201096.366	199467.559	199757.068	198677.070	198680.500
24	23	207656.434	206104.447	209820.363	208125.491	208453.365	207291.046	207295.249
25	24	216269.674	214676.530	218541.803	216781.621	217150.932	215902.003	215907.102
26	25	224878.354	223246.826	227260.799	225435.849	225849.671	224509.835	224515.940
27	26	233482.392	231815.250	235977.181	234088.125	234549.636	233114.404	233121.696
28	27	242081.680	240381.664	244690.701	242738.309	243250.734	241715.637	241724.217
29	28	250676.140	248946.150	253401.388	251386.448	251953.108	250313.498	250323.521
30	29	259265.708	257508.601	262109.072	260032.391	260656.587	258907.935	258919.578
31	30	267850.163	266068.926	270813.740	268676.136	269361.196	267498.881	267512.332
32	31	276429.652	274627.141	279515.045	277317.492	278066.738	276086.286	276101.741
33	32	285003.841	283183.216	288213.225	285956.591	286773.178	284670.169	284687.756
34	33	293572.990	291736.891	296908.304	294593.245	295480.897	293250.547	293270.510
35	34	302136.898	300288.319	305599.588	303227.298	304189.120	301827.305	301849.816
36	35	310695.427	308837.526	314287.237	311858.781	312898.199	310400.543	310425.797
37	36	319248.753	317384.449	322971.226	320487.696	321607.695	318970.615	318998.776
38	37	327797.050	325928.802	331651.457	329113.825	330317.826	327536.993	327568.310
39	38	336339.886	334470.616	340327.923	337737.433	339028.235	336099.791	336134.374
40	39	344877.468	343010.149	349000.227	346358.137	347738.994	344659.995	344698.049
41	40	353409.883	351547.259	357668.802	354975.868	356449.732	353216.538	353258.418
42	41	361937.203	360081.665				361770.522	361816.048
sequence		V093	V126	V131	V089	V006	V096	V097

a - The K quantum number notation is defined in the text below Eq. A.1.
b - all frequencies for J''>3 (unless otherwise marked) are experimental measurements with estimated uncertainty of 0.05 MHz. The frequencies for J''=0 to 3 are hyperfine removed frequencies evaluated by Koput.
c - calculated from a $J(J+1)$ power series fit to the sequence.

(b) v_b=0, m=1, $E_{\rm vib}$ = 8.4 cm^{-1}

K =		0	-1	1	2	-3	3
J'	J''						
1	0	8714.599					
2	1	17426.089	17131.350	17139.540			
3	2	26131.320	25696..960	25711.200	26102.200		
4	3	34827.319	34262.960	34285.420	34803.370	34746.730	34848.720
5	4	43511.298	42829.348	42862.701	43504.452	43433.533	43560.652
6	5	52181.118	51396.202	51443.858	52206.120	52119.989	52272.360
7	6	60834.588	59963.808	60029.019	60907.932	60806.734	69694.881
8	7	69470.354	68532.241	68618.612	69610.243	69493.349	78405.765
9	8	78087.660	77101.788	77212.768	78312.951	78180.079	87116.220
10	9	86686.556	85672.565	85811.546	87016.078	86866.748	95826.264
11	10	95267.825	94244.905	94414.872	95719.797	95553.457	104535.872
12	11	103832.990	102819.142	103022.546	104424.130	104240.089	113245.010
13	12	112384.189	111395.453	111634.362	113129.051	112926.739	121953.658
14	13	120923.957	119974.084	120250.061	121834.685	121613.360	130661.691
15	14	129455.041	128555.310	128869.183	130541.066	130300.215	139369.066
16	15	137980.105	137139.779	137491.243	139248.143	138986.740	148075.687
17	16	146501.448	145726.977	146115.877	147956.022	147673.312	156781.803
18	17	155021.205	154317.714	154742.833	156664.792	156360.035	165487.174
19	18	163541.133	162911.754	163371.518	165374.452	165046.706	174191.731
20	19	172061.977	171509.498	172001.511	174085.007	173733.277	182895.436
21	20	180584.517[a]	180110.821[a]	180632.418	182796.656	182419.917	191598.170
22	21	189109.455	188715.886	189263.550	191508.907	191106.420	200300.118
23	22	197636.492	197324.512	197894.577	200222.279	199792.672	209001.126
24	23	206165.981	205936.596	206525.339	208936.733	208478.868	217701.086
25	24	214697.618	214552.442	215155.261	217652.088	217164.881	226400.016
26	25	223231.128	223171.503	223783.952	226368.543	225850.618	235097.875
27	26	231766.341	231793.783	232411.044	235085.938	234535.866	243794.484
28	27	240302.835	240418.979	241036.217	243804.350	243220.575	252490.045
29	28	248840.351	249047.052	249659.091	252523.689	251904.576	261184.367
30	29	257378.635	257677.673	258279.428	261243.934	260587.611	269877.354
31	30	265917.341	266310.654	266896.862	269964.935	269269.306	278569.028
32	31	274456.286	274945.807	275511.130	278686.471	277949.280	287259.016
33	32	282995.138	283582.597	284122.057	287408.067	286626.968	295948.943
34	33	291533.591	292221.402	292729.120	296130.228	295302.132	304636.157
35	34	300071.437	300861.390	301332.036	304850.123	303973.342	313322.215
36	35	308608.768	309502.679	309930.935	b	312639.870	322006.608
37	36	317145.274	318145.064	318525.546	b	321299.883	330689.686
38	37	325680.738	326788.371	327115.335	b	329952.435	339370.491
39	38	334214.702	335432.305	335700.385	b	338594.440	348050.671
40	39	342747.571	344077.189	344280.710	b	347223.487	356728.558
41	40	351278.907	352722.522	352855.727	b	355835.853	
42	41	359808.783	361368.607	361425.535	b		
sequence		V107+X107	V101	V098	V010	V005	V012

a - calculated from a $J(J+1)$ power series fit to the sequence.
b - sequence too perturbed for confident assignment.

(c) v_b=0, m=-2, $E_{\rm vib}$ = 36.8 cm^{-1}

K =		0	-1	1	2	-3	3
J'	J''						
1	0	8712.440					
2	1	17424.730	17413.270	17404.820			
3	2	26137.030	26119.520	26109.160	25664.890		
4	3	34849.040	34825.770	34816.500	34225.420	34934.900	34961.090
5	4	43560.897[a,b]	43532.117	43527.498	42790.309	43668.171	43682.672
6	5	52272.451[a,b]	52238.073	52242.597	51360.437	52401.386	52392.272
7	6	60983.669[a,b]	60944.058	60962.565	59936.461	61134.338	61088.422
8	7	69694.485	69649.804	69687.625	68518.731	69866.924	69769.729
9	8	78404.856	78355.412	78417.926	77107.514	78599.133	78435.325
10	9	87114.738	87060.710	87153.379	85702.751	87330.888	87084.556
11	10	95824.056	95765.763	95893.514	94304.411	96062.185	95717.491
12	11	104532.714	104470.566	104637.665	102912.045	104793.013	104334.474
13	12	113240.653	113175.049	113384.876	111525.320	113523.228	112936.205
14	13	121947.700	121879.231	122134.022	120143.754	122252.995	121523.853
15	14	130653.851	130583.038	130883.320	128766.726	130982.052	130098.915
16	15	139358.532	139286.363	139631.255	137393.143	139710.254	138663.325
17	16	148061.901	147989.218	148376.092	146022.743	148437.799	147218.459
18	17	156763.754	156691.751	157116.399	154654.800	157164.567	155766.873
19	18	165463.564	165393.941	165850.049	163288.573	165890.628	164310.386
20	19	174161.002	174095.570	174575.538	171923.201	174615.757	172850.953
21	20	182855.593	182796.656	183291.443	180558.028[a]	183339.996	181390.412
22	21	191546.894	191497.178	191996.548	189192.720	192063.146	189930.316
23	22	200234.301	200197.129	200690.051	197826.437	200785.291	198472.093
24	23	208917.318	208896.491	209371.092	206458.663	209506.446	207017.068
25	24	217595.174	217595.174	218039.456	215089.004	218226.496	215566.166
26	25	226267.092	226293.413	226694.967	223717.009	226945.439	224120.207
27	26	234932.492[a]	234990.914	235337.649	232342.227	235663.096	232679.828
28	27	243590.630	243687.653	243967.818	240964.280	244379.611	241245.454
29	28	252240.796	252383.755	252585.612	249582.840	253094.867	249817.533
30	29	260882.339	261079.084	261192.583	258197.662	261808.735	258396.339
31	30	269514.732	269773.683	269788.424	266808.428	270521.346	266982.150
32	31	278137.623	278467.359	278374.254	275414.952	279232.105	275575.274
33	32	286750.691	287160.285	286951.163	284016.740	287942.047	284176.013
34	33	295354.251	295852.776	295520.181	292614.021	296650.575	292784.604
35	34	303947.944	304543.877	304081.558	301205.925	305357.256	301401.555
36	35	312532.293	313234.118	312636.900	309792.917	314062.421	310027.841
37	36	321107.766	321923.326	321186.461	318374.616	322765.830	318664.379
38	37	329675.596	330611.777	329732.148	326950.804	331468.033	327312.231
39	38	338235.598	339298.928	338273.907	335521.348	340168.379	335973.272
40	39	346789.247	347985.229	346813.067	344086.535	348867.181	344650.251
41	40	355337.165	356670.230	355350.283	352645.714	357564.298	353345.626
42	41				361199.462		362063.629
sequence		V119	V008	V180	V100	V024	V106+X106

a - calculated from a $J(J+1)$ power series fit to the sequence.
b - not measured since blended with another sequence.

(d) v_b=0, m=3L, E_{vib} = 80.3 cm^{-1}

K =		0	-1	1	2	3
J'	J''					
1	0	8722.070				
2	1	17444.100	17504.680	17448.710		
3	2	26166.190	26257.660	26172.870	26217.200	
4	3	34888.140	35011.480	34896.830	34956.060	35028.630
5	4	43609.928	43766.214	43620.571	43694.834	43785.654
6	5	52331.868	52522.551	52344.346	52433.136	52542.085
7	6	61053.565	61280.451[a]	61067.774	61171.238	61298.342
8	7	69775.192	70040.195	69790.946	69909.074	70054.280
9	8	78496.665	78801.997	78513.797	78646.527	78809.809
10	9	87218.054	87565.977	87236.266	87383.509	87564.879
11	10	95939.244	96332.237	95958.329	96120.050	96319.430
12	11	104660.269	105100.806	104679.971	104856.074	105073.483
13	12	113381.115	113871.438	113401.139	113591.533	113826.888
14	13	122101.880	122644.153	122121.912	122326.370	122579.897
15	14	130822.366	131418.379	130841.787	131060.695	131331.907
16	15	139542.464	140193.007	139561.260	139794.246[a]	140083.196
17	16	148262.442	148967.780	148280.088	148526.918	148833.657
18	17	156982.205	157741.459	156998.138	157259.087	157583.442
19	18	165701.855	166512.305	165715.596	165990.220	166332.231
20	19	174421.255	175278.820	174432.265	174720.445	175080.257
21	20	183140.586	184038.905	183148.090	183449.784	183827.235
22	21	191859.411	192789.989	191863.107	192178.078	192573.044
23	22	200577.940[a]	201529.781	200577.113[a]	200905.313	201317.746
24	23	209296.343	210255.519	209290.275	209631.511	210061.385
25	24	218014.630	218964.185	218002.461	218356.609	218803.854
26	25	226732.746	227652.903	226713.682	227080.543	227544.975
27	26	235450.617	236318.690	235423.772	235803.211	236284.963
28	27	244168.331	244958.968	244132.818	244524.636	245023.577
29	28	252885.887	253571.479	252840.703	253244.748	253760.717
30	29	261603.311	262154.856	261547.430	261963.534	262496.451
31	30	270320.529	270708.260	270253.052	270680.897	271231.791
32	31	279037.620	279232.105	278957.203	279396.720	279962.773
33	32	287754.622	287727.766	287660.097	288110.813	288694.607
34	33	296471.734	296199.254	296361.967	296824.183	297424.153
35	34	305188.310	304649.763	305062.223	305535.487	306152.116
36	35	313904.998	313084.650	313760.953	314244.899	314878.144
37	36	322621.009	321509.320	322458.384	322952.760	323602.325
38	37	331337.282	329929.323	331154.531	331658.794	332324.862
39	38	340052.790	338348.803	339848.777	340363.324	b
40	39	348767.954	346771.793	348541.475	349065.775	b
41	40	357482.199	355200.745	357232.817	357766.597	b
42	41					
sequence		V017	V137	V082	V030	V040

a - calculated from a $J(J+1)$ power series fit to the sequence.
b - not measured owing to the appearance of additional small doubling and blending with another sequence.

(e) v_b=0, m=3U, E_{vib} = 79.7 cm^{-1}					v_b=0, m=4, 140.6 cm^{-1}	v_b=0, m=-5, 217.5 cm^{-1}
K =		0	-1	2	0	0
J'	J''					
1	0	8722.930			8737.510	8755.450
2	1	17445.790	17454.140		17474.880	17510.750
3	2	26168.670	26181.160	26217.200	26212.280	26265.930
4	3	34891.510	34907.990	34956.060	34949.500	35021.170
5	4	43614.169	43634.803	43694.834	43686.558	43776.052
6	5	52337.008	52361.126	52433.136	52423.467	52530.822
7	6	61059.598	61087.316	61171.238	61160.109	61285.235
8	7	69782.154	69813.257	69909.074	69896.532	70039.333
9	8	78504.575	78538.859	78646.527	78632.611	78793.106
10	9	87226.921	87264.103	87383.509	87368.415	87546.486
11	10	95949.108	95988.904	96120.050	96103.815	96299.372
12	11	104671.232	104713.296	104856.074	104838.731	105051.763
13	12	113393.159	113437.179	113591.533	113573.462	113803.590
14	13	122115.041	122160.503	122326.370	122307.385	122554.987
15	14	130836.609	130883.320	131060.695	131040.907	131305.539
16	15	139558.099	139605.335	139793.874[a]	139773.828	140055.353
17	16	148279.376	148326.896	148526.393	148506.076	148804.383
18	17	157000.493	157047.593	157258.419	157237.942	157552.953
19	18	165721.632	165767.724	165989.446	165969.028	166300.585
20	19	174442.476	174486.974	174719.575	174699.344	175047.384
21	20	183163.236	183205.461	183448.801	183429.044	183793.009
22	21	191883.717	191922.912	192176.926	192157.781	192537.886
23	22	200604.112	200639.521	200903.965	200885.786	201281.751[a,b]
24	23	209324.337	209355.240	209630.000	209612.881	210024.510[a,b]
25	24	218044.534	218069.900	218354.946	218339.144	218766.186
26	25	226764.650	226783.590	227078.696	227064.506	227506.674
27	26	235484.635	235496.154	235801.163	235788.832	236245.972
28	27	244204.559	244207.596	244522.386	244512.199	244984.016
29	28	252924.508	252917.912	253242.286	253234.561	253720.771
30	29	261644.369	261626.983	261960.792	261955.843	262456.197
31	30	270364.327	270334.789	270677.907	270676.015	271190.307
32	31	279084.315	279041.258	279393.357	279395.008	279922.741
33	32	287804.144	287746.709[a]	288107.240	288112.677	288653.970
34	33	296524.473	296450.663	296820.277	296829.834	297383.564
35	34	305244.523	305153.091	305531.426	305545.340	306111.655
36	35	313964.548	313854.002	314240.338	314259.408	314838.069
37	36	322684.235	322553.329	322947.835	322972.358	323562.679
38	37	331404.493	331251.686	331653.583	331683.823	332285.799
39	38	340124.133	339947.987	340357.652	340394.140	341007.079
40	39	348843.625	348642.878	349059.672	349102.921	349726.678
41	40	357562.542	357335.976	357760.089	357810.572	358444.316
42	41					
sequence		V018	V020	V029	V025	V142

a - calculated from a $J(J+1)$ power series fit to the sequence.
b - not measured owing to blending with another sequence.

(f) v_b=0, m=0, $E_{\rm vib}$ = 182.2 cm^{-1}

K =		0	1L	1U
J'	J''			
1	0	8670.610		
2	1	17340.960	17188.670	17510.450
3	2	26011.020	25782.370	26265.980
4	3	34680.440	34376.120	35019.950
5	4	43349.173	42969.421	43774.035
6	5	52016.906	51562.541	52527.823
7	6	60683.541	60155.123	61280.888
8	7	69348.900	68747.151	70033.282
9	8	78012.766	77338.547	78784.866
10	9	86674.929	85929.270	87535.510
11	10	95335.299	94519.235	96285.169
12	11	103993.608	103108.301	105033.678
13	12	112649.673	111696.508	113781.001
14	13	121303.479	120283.613	122526.957
15	14	129954.672	128870.034	131271.662
16	15	138603.026	137454.881	140014.495
17	16	147248.768[a]	146038.531	148755.988
18	17	155891.279	154621.245	157495.713
19	18	164530.700	163202.325	166233.670
20	19	173166.705	171782.207	174969.640
21	20	181799.215	180360.456[a]	183703.515
22	21	190428.000	188937.343	192435.609
23	22	199053.039	197512.392	201165.038
24	23	207674.136	206085.904	209892.319
25	24	216291.199	214657.696	218617.180
26	25	224904.062	223227.702	227339.566
27	26	233512.629	231795.913	236059.320
28	27	242116.760	240362.160	244776.394
29	28	250716.407	248926.484	253490.700
30	29	259311.510	257488.850	262201.998
31	30	267901.799	266049.115	270910.320
32	31	276487.436	274607.275	279615.511
33	32	285068.035	283163.366	288317.636
34	33	293644.004	291717.164	297016.541
35	34	302214.882	300268.707	305712.236
36	35	310780.705	308817.997	314404.000
37	36	319341.519	317365.129	323092.435
38	37	327897.500	325909.693	331777.190[a]
39	38	336448.316	334451.713	340458.290
40	39	344993.807	342991.511	349135.442
41	40	353534.354	351528.890	357808.901
42	41	362069.899	360063.601	
sequence		V094	V127	V132

a - calculated from a $J(J+1)$ power series fit to the sequence.

Table A.6. Line list for CH_3NCO.

Frequency (MHz)	Error (MHz)	Log(Int) [a]	DR [b]	E_{low} cm^{-1}	g_{upp} [c]	TAG [d]	QNFMT [e]	QN′ [f]				QN″ [g]			
60688.210	0.0500	-5.0017	3	6.0737	15	01	404	7	0	7	0	6	0	6	0
69353.880	0.0500	-4.8323	3	8.0980	17	01	404	8	0	8	0	7	0	7	0
78017.953	0.0500	-4.6840	3	10.4114	19	01	404	9	0	9	0	8	0	8	0
86680.190	0.0500	-4.5525	3	13.0138	21	01	404	10	0	10	0	9	0	9	0
95340.443	0.0500	-4.4348	3	15.9051	23	01	404	11	0	11	0	10	0	10	0
103998.481	0.0500	-4.3284	3	19.0854	25	01	404	12	0	12	0	11	0	11	0
112654.059	0.0500	-4.2317	3	22.5544	27	01	404	13	0	13	0	12	0	12	0
121307.237	0.0500	-4.1434	3	26.3121	29	01	404	14	0	14	0	13	0	13	0

Table following the format of the JPL catalog (see Sect. A.2).
a - Base 10 logarithm of the integrated intensity in units of nm^2 MHz at 300 K.
b - Degrees of freedom in the rotational partition function.
c - Upper state degeneracy.
d - Species tag or molecular identifier.
e - Format of the quantum numbers.
f - Quantum numbers for the upper state.
g - Quantum numbers for the lower state.
This table is available in its entirety at the CDS. A portion is shown here for guidance regarding its form and content.

Table A.7. Comparison of rotational transition frequencies for CH_3NCO between those reported in Halfen et al. (2015) and in this work.

J'	K'_a	K'_c	J''	K''_a	K''_c	symm.	m	Halfen et al. (2015)	This work	Difference
								measured		
7	-1	7	6	-1	6	E	1	60029.044	60029.019	0.025
7	1	6	6	1	5	A	0	60160.932	60162.076	−1.144[a]
7	0	7	6	0	6	A	0	60688.191	60688.210	−0.019
7	0	7	6	0	6	E	1	60833.422	60834.588	−1.166[a]
7	1	7	6	1	6	A	0	61260.729	61260.734	−0.001
8	-1	8	7	-1	7	E	1	68617.550	68618.612	−1.062[a]
8	1	7	7	1	6	A	0	68753.890	68755.025	−1.135[a]
8	0	8	7	0	7	A	0	69353.888	69353.880	0.008
8	0	8	7	0	7	E	1	69469.196	69470.354	−1.154[a]
8	1	8	7	1	7	A	0	70009.179	70010.208	−1.029[a]
9	1	8	8	1	7	E	1	77107.478[b]	77101.788	5.690
9	-1	9	8	-1	8	E	1	77211.707	77212.768	−1.061[a]
9	1	8	8	1	7	A	0	77347.355	77347.425	−0.070
9	0	9	8	0	8	A	0	78017.932	78017.953	−0.021
9	0	9	8	0	8	E	1	78087.673	78087.660	0.013
9	1	9	8	1	8	A	0	78758.868	78758.849	0.019
10	-1	10	9	-1	9	E	1	85811.557	85811.546	0.011
10	1	9	9	1	8	A	0	85938.967	85938.962	0.005
10	0	10	9	0	9	A	0	86680.195	86680.190	0.005
10	0	10	9	0	9	E	1	86686.575	86686.556	0.019
10	1	10	9	1	9	A	0	87506.605	87506.607	−0.002
								calculated		
8	1	7	7	1	6	E	1	68536.76[c]	68532.241	4.519
10	1	9	9	1	8	E	1	85679.63[c]	85672.565	7.065
11	1	10	10	1	9	E	1	94253.49[c]	94244.905	8.585
12	1	11	11	1	10	E	1	102829.92[c]	102819.142	10.778

Notes.
[(a)]One of seven lines from Halfen et al. (2015) showing a ≥1 MHz frequency shift relative to the present work. Other lines in the same transition sequences measured in Halfen et al. (2015) do not seem to be affected.
[(b)]This is a bona fide line in our experimental spectrum but our assignment is m=−2, K=2 with measured frequency of 77107.514 MHz.
[(c)]Prediction in Halfen et al. (2015) based on the misassigned 77107.478 MHz line. There are no lines in our experimental spectrum at these frequencies, and the actual K=+1, m=1 lines are at significantly lower frequencies.

Table A.8. Calculated frequencies and relative intensities of nuclear quadrupole splitting components for the K_a=0,1,2 ground state (v_b=0, m=0) rotational transitions of CH_3NCO.

	K = 0			K = 1L			K = 1U			K = 2L			K = 2U	
F' - F''	ν^a / MHz	$I_{rel}{}^b$	F' - F''	ν / MHz	I_{rel}	F' - F''	ν / MHz	I_{rel}	F' - F''	ν / MHz	I_{rel}	F' - F''	ν / MHz	I_{rel}
J = 1 - 0														
0 - 1	8669.943	0.1111												
2 - 1	8671.222	0.5555												
1 - 1	8672.076	0.3334												
J = 2 - 1														
1 - 1	17341.104	0.0833	1 - 0	17189.333	0.1111	1 - 0	17503.509	0.1111						
1 - 2	17341.957	0.0056	1 - 2	17189.916	0.0056	1 - 2	17504.205	0.0056						
3 - 2	17342.465	0.4667	3 - 2	17190.192	0.4667	3 - 2	17504.436	0.4667						
2 - 1	17342.526	0.2500	1 - 1	17190.305	0.0833	1 - 1	17504.669	0.0833						
1 - 0	17343.237	0.1111	2 - 2	17190.690	0.0833	2 - 2	17504.853	0.0833						
2 - 2	17343.379	0.0833	2 - 1	17191.079	0.2500	2 - 1	17505.317	0.2500						
J = 3 - 2														
2 - 2	26012.000	0.0370	2 - 2	25784.511	0.0370	2 - 2	26255.928	0.0370	2 - 1	26037.145	0.2000	2 - 1	26037.736	0.2000
2 - 3	26012.914	0.0011	2 - 3	25785.008	0.0011	2 - 3	26256.344	0.0011	3 - 3	26037.653	0.0370	3 - 3	26038.244	0.0370
4 - 3	26013.246	0.4286	4 - 3	25785.272	0.4286	2 - 1	26256.576	0.2000	4 - 3	26037.653	0.4286	4 - 3	26038.244	0.4286
3 - 2	26013.280	0.2963	2 - 1	25785.285	0.2000	4 - 3	26256.578	0.4286	2 - 3	26037.653	0.0011	2 - 3	26038.244	0.0011
2 - 1	26013.422	0.2000	3 - 2	25785.527	0.2963	3 - 2	26256.831	0.2963	2 - 2	26038.567	0.0370	3 - 2	26039.158	0.2963
3 - 3	26014.194	0.0370	3 - 3	25786.025	0.0370	3 - 3	26257.247	0.0370	3 - 2	26038.567	0.2963	2 - 2	26039.158	0.0370
J = 4 - 3														
3 - 3	34682.204	0.0208	3 - 3											
3 - 4	34683.153	0.0003	3 - 4	34379.823	0.0003	3 - 4	35008.150	0.0003	3 - 3	34716.569	0.0208	3 - 3	34718.047	0.0003
5 - 4	34683.402	0.4074	5 - 4	34380.045	0.4074	5 - 4	35008.351	0.4074	3 - 4	34716.569	0.0003	3 - 4	34718.047	0.0208
4 - 3	34683.424	0.3125	3 - 2	34380.086	0.2381	3 - 2	35008.384	0.2381	5 - 4	34716.669	0.4074	5 - 4	34718.146	0.4074
3 - 2	34683.484	0.2381	4 - 3	34380.160	0.3125	4 - 3	35008.463	0.3125	4 - 3	34717.057	0.3125	4 - 3	34718.534	0.0208
4 - 4	34684.372	0.0208	4 - 4	34380.912	0.0208	4 - 4	35009.132	0.0208	4 - 4	34717.057	0.0208	4 - 4	34718.534	0.3125
J = 5 - 4														
4 - 4	43351.569	0.0133	4 - 4	42973.421	0.0133	4 - 4	43758.741	0.0133	4 - 4	43394.804	0.0133	4 - 4	43397.758	0.0133
4 - 5	43352.539	0.0001	4 - 5	42974.288	0.0001	4 - 5	43759.523	0.0001	4 - 5	43395.192	0.0001	4 - 5	43398.145	0.0001
6 - 5	43352.740	0.3939	6 - 5	42974.477	0.3939	6 - 5	43759.694	0.3939	4 - 3	43395.292	0.2593	4 - 3	43398.245	0.2593
5 - 4	43352.755	0.3200	4 - 3	42974.511	0.2593	4 - 3	43759.723	0.2593	6 - 5	43395.312	0.3939	6 - 5	43398.265	0.3939
4 - 3	43352.788	0.2593	5 - 4	42974.540	0.3200	5 - 4	43759.755	0.3200	5 - 4	43395.515	0.3200	5 - 4	43398.468	0.3200
5 - 5	43353.725	0.0133	5 - 5	42975.407	0.0133	5 - 5	43760.537	0.0133	5 - 5	43395.903	0.0133	5 - 5	43398.856	0.0133
J = 6 - 5														
5 - 5	52019.907	0.0093	5 - 5	51567.406	0.0093	5 - 5	52509.526	0.0093	5 - 5	52072.829	0.0093	5 - 5	52077.994	0.0093
5 - 6	52020.892	0.0001	5 - 6	51568.335	0.0001	5 - 6	52510.369	0.0001	5 - 6	52073.419	0.0001	5 - 6	52078.584	0.0001
7 - 6	52021.060	0.3846	7 - 6	51568.499	0.3846	7 - 6	52510.517	0.3846	7 - 6	52073.539	0.3846	7 - 6	52078.704	0.3846
6 - 5	52021.071	0.3241	5 - 4	51568.525	0.2727	5 - 4	52510.540	0.2727	5 - 4	52073.540	0.2727	5 - 4	52078.705	0.2727
5 - 4	52021.092	0.2727	6 - 5	51568.538	0.3241	6 - 5	52510.555	0.3241	6 - 5	52073.660	0.3241	6 - 5	52078.824	0.3241
6 - 6	52022.056	0.0093	6 - 6	51569.467	0.0093	6 - 6	52511.398	0.0093	6 - 6	52074.250	0.0093	6 - 6	52079.415	0.0093
J = 7 - 6														
6 - 6	60687.022	0.0068	6 - 6	60160.922	0.0068	6 - 6	61259.710	0.0068	6 - 6	60750.459	0.0068	6 - 6	60758.718	0.0068
6 - 7	60688.018	0.0000	6 - 7	60161.890	0.0000	6 - 7	61260.590	0.0000	6 - 7	60751.170	0.0000	6 - 7	60759.428	0.0000
8 - 7	60688.163	0.3778	8 - 7	60162.034	0.3778	8 - 7	61260.721	0.3778	8 - 7	60751.284	0.3778	8 - 7	60759.542	0.3778
7 - 6	60688.171	0.3265	6 - 5	60162.054	0.2820	6 - 5	61260.739	0.2821	6 - 5	60751.290	0.2821	6 - 5	60759.548	0.2821
6 - 5	60688.186	0.2821	7 - 6	60162.060	0.3265	7 - 6	61260.746	0.3265	7 - 6	60751.361	0.3265	7 - 6	60759.619	0.3265
7 - 7	60689.167	0.0068	7 - 7	60163.028	0.0068	7 - 7	61261.627	0.0068	7 - 7	60752.072	0.0068	7 - 7	60760.330	0.0068
J = 8 - 7														
7 - 7	69352.717	0.0052	7 - 7	68753.883	0.0052	7 - 7	70009.183	0.0052	7 - 7	69427.576	0.0052	7 - 7	69439.955	0.0052
7 - 8	69353.721	0.0000	7 - 8	68754.877	0.0000	7 - 8	70010.088	0.0000	7 - 8	69428.365	0.0000	7 - 8	69440.743	0.0000
9 - 8	69353.849	0.3725	9 - 8	68755.005	0.3725	9 - 8	70010.205	0.3726	9 - 8	69428.471	0.3726	9 - 8	69440.848	0.3725
8 - 7	69353.855	0.3281	7 - 6	68755.021	0.2889	7 - 6	70010.219	0.2889	7 - 6	69428.479	0.2889	7 - 6	69440.856	0.2889
7 - 6	69353.866	0.2889	8 - 7	68755.024	0.3281	8 - 7	70010.223	0.3281	8 - 7	69428.524	0.3281	8 - 7	69440.902	0.3281
8 - 8	69354.860	0.0052	8 - 8	68756.018	0.0052	8 - 8	70011.128	0.0052	8 - 8	69429.313	0.0052	8 - 8	69441.690	0.0052
J = 9 - 8														
8 - 8	78016.793	0.0041	8 - 8	77346.206	0.0041	8 - 8	78757.837	0.0041	8 - 8	78104.085	0.0041	8 - 8	78121.752	0.0041
8 - 9	78017.805	0.0000	8 - 9	77347.220	0.0000	8 - 9	78758.761	0.0000	8 - 9	78104.927	0.0000	8 - 9	78122.593	0.0000
10 - 9	78017.918	0.3684	10 - 9	77347.334	0.3684	10 - 9	78758.866	0.3684	10 - 9	78105.026	0.3684	10 - 9	78122.692	0.3685
8 - 7	78017.924	0.3292	8 - 7	77347.347	0.2941	8 - 7	78758.877	0.2941	8 - 7	78105.033	0.2941	8 - 7	78122.699	0.2941
9 - 8	78017.932	0.2941	9 - 8	77347.348	0.3292	9 - 8	78758.879	0.3292	9 - 8	78105.064	0.3292	9 - 8	78122.730	0.3292
9 - 9	78018.935	0.0041	9 - 9	77348.361	0.0041	9 - 9	78759.803	0.0041	9 - 9	78105.906	0.0041	9 - 9	78123.571	0.0041

Notes.
[a]Calculated frequency with uncertainty estimated at 5 kHz.
[b]Relative intensity of a given hyperfine component such that the sum over all components for this rotational transition is unity.

Appendix B: Astrophysical methods

Appendix B.1: The Orion BN/KL region

Orion BN/KL (Becklin-Neugebauer/Kleinmann-Low; Becklin & Neugebauer 1967; Kleinmann & Low 1967) is the closest (about 414 pc; Menten et al. 2007) region exhibiting several processes related to young stellar objects (YSOs) and high-mass star formation (Genzel & Stutzki 1989). This region is located at the core of the Orion molecular cloud 1 (OMC1) which lies behind the Orion Nebula cluster (O'Dell 2001). Infrared facilities and radio telescopes can observe inside dusty regions where the formation of stars or their associated violent phenomena take place, providing very useful information about these processes. Near- and mid-IR subarcsecond resolution imaging and (sub)millimetre interferometric observations have identified the main sources of luminosity, heating, and dynamics in the region. At first, IRc2 was proposed as the main source of luminosity, heating, and dynamics within the region (Wynn-Williams et al. 1984). However, the detection of two radio continuum sources, *B* (coincident with the *BN* object which was resolved with high spatial resolution at 7 mm; Rodríguez et al. 2009) and *I* (centroid of the SiO masers and located 0.5″ south of IRc2; Menten & Reid 1995) revealed that the intrinsic IR luminosity of IRc2 ($L \sim 1000 L_{\odot}$) is only a fraction of the luminosity of the entire system ($1{\times}10^5 L_{\odot}$; Gezari et al. 1998). The radio continuum emission of the IR source *n* was also identified by Menten & Reid (1995) (3″ south-west from source *I*), suggesting this source as another precursor of the large-scale phenomena. In addition, several IR and millimetre continuum sources have been identified (Shuping et al. 2004; Wu et al. 2014). Thus, the core of Orion KL contains at least three self-luminous objects (protostars), the compact HII regions *I*, *n* (see Figs. 3 and B.3), and *BN*; these sources are within a region of ∼10″ (∼0.02 pc). Their proper motions reveal that they run away from a common region (Gómez et al. 2005). Different scenarios, as well as the formation of high-mass stars, have been proposed to explain the complexity of this source. An explosion of a multistar system (sources *I*, *n*, and *BN*) that took place ∼500 years ago has been proposed as the main factor responsible for most of the Orion KL gas components (Zapata et al. 2011).

The different gas components show distinct physical and chemical properties, which can be identified even with single-dish telescopes by a characteristic systemic velocity (Blake et al. 1987; Schilke et al. 2001; Tercero et al. 2010). Classically, these components have been called *Hot Core*, a hot, ∼200-300 K, and dense clump rich in complex organic saturated N-bearing species such as CH_3CH_2CN, characterized by $\Delta v_{FWHM} \sim 5$-$15\,\mathrm{km\,s^{-1}}$ and $v_{\rm LSR} \sim 5$-$7\,\mathrm{km\,s^{-1}}$; *Extended Ridge*, the host, quiescent, and relatively cold, ∼60 K ambient cloud rich in simple species such as CS or HCN, emitting lines with $\Delta v_{FWHM} \sim 3$-$4\,\mathrm{km\,s^{-1}}$ and $v_{\rm LSR} \sim 8$-$9\,\mathrm{km\,s^{-1}}$; *Compact Ridge*, a warm, ∼150 K, and compact clump rich in organic saturated O-rich species such as CH_3OCOH or CH_3OCH_3, whose spectral features are characterized by $\Delta v_{FWHM} \sim 2$-$3\,\mathrm{km\,s^{-1}}$ and $v_{\rm LSR} \sim 7$-$8\,\mathrm{km\,s^{-1}}$; and *Plateau*, molecular outflows presenting typical shock chemistry with molecules such as SO or SiO (Goicoechea et al. 2015); the low velocity flow (oriented along the SW-NE direction and probably driven by source *I*) is characterized by lines with $\Delta v_{FWHM} \sim 20\,\mathrm{km\,s^{-1}}$ and $v_{\rm LSR} \sim 5$-$6\,\mathrm{km\,s^{-1}}$, whereas the high-velocity flow (oriented along the SE-NW direction and whose origin could be the explosive event caused by the dynamical decay of a multi-star system briefly described above) presents lines with Δv_{FWHM} as wide as $150\,\mathrm{km\,s^{-1}}$ and $v_{\rm LSR} \sim 10\,\mathrm{km\,s^{-1}}$. Interferometric observations have shown other cloud components inside Orion BN/KL such as the millimetre continuum sources MM2, MM4 (which corresponds approximately to Position B, see Figs. 3 and B.3), MM5, and MM6 (Wu et al. 2014). In addition, these latter observations reveal the hot core to be a collection of very dense and hot clumps presenting different chemistry and radial velocities (Favre et al. 2011; Tercero et al. 2015). Position A of Figs. 3 and B.3 is located in the middle of the hot core clumpy structure.

Appendix B.2: Observations

Appendix B.2.1: IRAM 30m

We performed a sensitive, fully single side band reduced, line survey towards Orion IRc2 with the IRAM 30m telescope over broad frequency ranges (total frequency coverage of ∼168 GHz; Tercero et al. 2010). Our main goal was to obtain a deep insight into the molecular content and chemistry of Orion BN/KL and to improve our knowledge of its prevailing physical conditions. It also allows us to search for new molecular species and new isotopologues, as well as the rotational emission of vibrationally excited states of molecules already known to exist in this source (see Sect. B.3 and main text).

The line survey was performed over three millimetre-wave windows (3, 2, and 1.3 mm, covering frequency ranges 80−115.5 GHz, 130−178 GHz, and 197−281 GHz, respectively) with the IRAM 30m telescope. The observations were carried out between September 2004 and January 2007 pointing toward the IRc2 source at $\alpha_{2000.0} = 5^h35^m14\overset{s}{.}5$, $\delta_{2000.0} = -5°22'30\overset{''}{.}0$. Four SiS receivers were used simultaneously, with image sideband rejections within ∼13 dB (1.3 mm receivers), 12−16 dB (2 mm receivers), and 20−27 dB (3 mm receivers). The observations were performed using the wobbler switching mode with a beam throw in azimuth of ±120″. No contamination from the off position affected our observations, except for a marginal amount at the lowest elevations (25°) for molecules showing low-*J* emission along the ambient molecular cloud. System temperatures were in the range of 100−800 K from the lowest to the highest frequencies. For the spectra between 172−178 GHz, the system temperature was significantly higher, 1000−4000 K, owing to proximity of the atmospheric water line at 183.31 GHz. The intensity scale was calibrated using the atmospheric transmission model (ATM; Pardo et al. 2001; Cernicharo 1985). Focus and pointing were checked every 1−2 hours on planets or nearby quasars. Backends provided a spectral resolution of 1−1.25 MHz. The half power beam width (HPBW) of the 30m telescope ranged from 31″ to 9″ from 80 to 280 GHz (HPBW[arcsec]=2460/Freq.[GHz]). The data were reduced using the GILDAS package[1] checking for image sideband contamination and fitting and removing 0−1 order baselines. Figures using these data are shown in main beam temperature (T_{MB}).

Appendix B.2.2: ALMA SV

The ALMA Science Verification (SV) data were taken in January 2012 towards the IRc2 region in Orion. The observations were carried out with 16 antennas of 12 m in the frequency range from 213.715 to 246.627 GHz (Band 6). The primary beam was ∼27″. Spectral resolution was 0.488 MHz (∼0.64 km s^{-1} in the observed frequency range). The observations were centred on coordinates: $\alpha_{J2000} = 05^h35^m14\overset{s}{.}35$, $\delta_{J2000} = -05°22'35\overset{''}{.}00$. The

[1] http://www.iram.fr/IRAMFR/GILDAS

CASA software[2] was used for initial processing, and then the visibilities were exported to the GILDAS package for further analysis. The synthesized beam ranged from 2.″00×1.″48 with a PA of 176° at 214.0 GHz to 1.″75×1.″29 with a PA of 164° at 246.4 GHz. The brightness temperature to flux density conversion factor is 9 K for 1 Jy per beam. The continuum emission was subtracted in the maps by carefully selecting line-free channels.

Appendix B.3: Astronomical model

Appendix B.3.1: Orion KL

Frequency predictions and intensities reported in this work were implemented in MADEX (Cernicharo 2012) to model the emission of CH_3NCO and to search for it toward Orion KL. MADEX is an excitation and radiative transfer code which includes more than 5200 molecular species with accurate spectroscopy. To derive the physical parameters shown in Table B.1, we performed a model that reproduces more line profiles more accurately from transitions covering a wide energy range within a ∼30% of the uncertainty in line intensity (red lines in Figs. 2 and B.1).

Owing to the lack of collisional rates for this molecule, we used LTE approximation. Nevertheless, taking into account the physical conditions of the considered components of the cloud (see Table B.2), we expect that this approximation works reasonably well (see e.g. Fortman et al. 2012). For each spectral component, we assume uniform physical conditions of the cloud (line width, radial velocity, and source size with uniform brightness temperature and optical depth over this size), which we choose by taking into account the parameters obtained from Gaussian fits of the line profiles and the emission shown by the ALMA maps. To fit the IRAM 30m lines, we also considered the beam coupling effects adding the offset position with respect to IRc2 (the pointing position). Corrections for beam dilution are also applied for each line depending on the different beam sizes at different frequencies. Therefore, we fixed all of the above parameters leaving only the rotational temperature and the column density as free parameters for each component. In order to determine the uncertainty of the values of column density and of temperature, we ran several models varying only the values for these parameters and fixing the rest. To fit the ALMA data we extracted the averaged spectrum over 5×5 pixels (∼1″×1″) around Position A and Position B (see Figs. 3 and B.3). To derive the column densities and relative abundances of the species shown in Table B.1, we adopted the same model of CH_3NCO for each position varying the column density for each one of the species of Table B.1. In Fig. B.1, a model containing all species already studied in the IRAM 30m survey is included (cyan line). The molecules considered in the models and references to their modelling and analysis are given in Table B.3. This table also summarizes the works performed to date based on the 30m data and devoted to mitigating the number of unidentified lines in the IRAM 30m survey of Orion (especially those in collaboration with spectroscopy laboratories), to searching for new molecular species in interestelar clouds, and to improving the knowledge of the physical-chemical properties of Orion KL.

Appendix B.3.2: Sgr B2(N)

We have searched in published line surveys of Sgr B2 and W51 for CH_3NCO. We find that 21 unidentified features above 13σ found in Sgr B2 by Belloche et al. (2013) can be unambiguously assigned to CH_3NCO. However, in the PRIMOS data (Neill et al. 2012) of the same source the assignment is not obvious. CH_3NCO was also reported in Sgr B2 during the submission process of this work (Halfen et al. 2015). We used MADEX and the public data of Sgr B2(N) provided by Belloche et al. (2013) to derive the rotational temperature and column density of methyl isocyanate in this source (see Fig. B.2, red line). We find that the two hot ($T_{rot} = 200$ K) and compact ($d_{sou} \simeq 2''$) components derived by Belloche et al. (2013) for HNCO are enough to reproduce all lines that appear at 3 mm. We derive column densities of $N = 5\times10^{17}$ cm^{-2} for the 63 km s^{-1} component and 3×10^{17} cm^{-2} for the second component at 73 km s^{-1} (assuming $\Delta v_{FWHM} = 7$ km s^{-1}, see Belloche et al. 2013).

In W51 (Pulliam et al. 2012), another well-known hot core with similar molecular content than Orion, we do not find an obvious detection in the data, because the lines are weaker owing to the higher distance of W51 compared to Orion.

Methyl isocyanate turns out to be one of the prominent molecules in hot cores and it is surprising to realize that it is present in many line surveys. It was only the lack of suitable laboratory data delayed its discovery. In the present work it is the close collaboration between astronomers and molecular physicists that has made such detailed characterization of this new molecular species possible.

Appendix B.4: Spatial distribution in Orion

The spatial distribution of several molecules detected in Orion KL is shown in Figs. 3 and B.3. Despite the lack of short spacing data required for completion of the possible extended emission of some of these species (see e.g. CH_3OH or DCN), we can obtain an overview of the main cores that host these species. Moreover, the discussion has to address the large differences in energies of the upper level for the transitions involved in those maps (it is not possible to find transitions with similar energies of, for instance, DCN and HC_3N v_7=1 between 213.7−247.5 GHz, the coverage of the ALMA SV data). In addition, owing to the extreme complexity of Orion KL, it is not straightforward to find lines free of blending with other species in the whole region: many lines of a large variety of molecules that appear unblended in some cores, overlap with lines of other species in the average spectrum of the region. This makes it more difficult to derive maps of lines involving transitions with uniform upper level energies. Nevertheless, by taking these restrictions into account, the discussion can be focused on the main differences/similarities found for the different "families" of molecules.

As we have pointed out in the main text, we note a similar spatial distribution for CH_3NCO, NH_2CHO, and HNCO. The main differences of these maps are a larger extension of HNCO due to its higher abundance and the lack of the clump in the NW of position B for NH_2CHO; in addition, CH_3NCO does not emit in this region, whereas HNCO and NH_2CHO show some emission at the position of the compact ridge. It is worth noting that these species are the only three detected in Orion KL containing Nitrogen, Oxygen, Carbon, and Hydrogen together.

Following with the compact ridge, this component is the main host of CH_3OCH_3, CH_3OCOH, and CH_2OCH_2, all of them organic compounds containing oxygen. Molecules that we could naively think that are related with them, such as CH_3CH_2OH, CH_3COCH_3, CH_3COOH, $OHCH_2CH_2OH$, and CH_2OHCHO, present a completely different spatial distribution (Guélin et al. 2008; Peng et al. 2012, 2013; Widicus Weaver & Friedel 2012; Friedel & Widicus Weaver 2012; Brouillet et al. 2015; Feng et

[2] http://casa.nrao.edu

Table B.1. Molecular abundances in Orion and in Comet 67P/Churyumov-Gerasimenko

Species	Comet	Orion Position A		Orion Position B	
	Abundance rel. to H_2O	Column density (cm^{-2})	Abundance rel. to H_2O (×100)	Column density (cm^{-2})	Abundance rel. to H_2O (×100)
H_2O^a	100	$(3 \pm 1)\times10^{19}$	100	$(2.0 \pm 0.6)\times10^{19}$	100
HCN^a	0.9	$(4 \pm 1)\times10^{17}$	1.3	$(2.0 \pm 0.6)\times10^{17}$	1.0
CO^b	1.2	$(4 \pm 1)\times10^{19}$	130	$(1.0 \pm 0.3)\times10^{19}$	50
CH_3NH_2	0.6	$\leq(4 \pm 1)\times10^{15}$	≤0.01	$(4 \pm 1)\times10^{15}$	0.02
CH_3CN^c	0.3	$(7 \pm 3)\times10^{16}$	0.2	$(1.0 \pm 0.3)\times10^{17}$	0.5
HNCO	0.3	$(1.0 \pm 0.3)\times10^{17}$	0.3	$(7 \pm 3)\times10^{16}$	0.35
CH_3CHO	0.5	$(1.6 \pm 0.5)\times10^{15}$	0.005	$(1.4 \pm 0.3)\times10^{15}$	0.0075
$HCONH_2$	1.8	$(4 \pm 1)\times10^{15}$	0.01	$(7 \pm 3)\times10^{14}$	0.0035
$CH_3CH_2NH_2{}^d$	0.3	$\leq(4 \pm 1)\times10^{14}$	≤0.001	$\leq(2 \pm 1)\times10^{14}$	≤0.001
CH_3NCO	1.3	$(7 \pm 3)\times10^{15}$	0.02	$(4 \pm 1)\times10^{15}$	0.02
CH_3COCH_3	0.3	$(1.4 \pm 0.4)\times10^{16}$	0.04	$(1.1 \pm 0.3)\times10^{16}$	0.055
$CH_3CH_2CHO^d$	0.1	$\leq(1.0 \pm 0.3)\times10^{15}$	≤0.003	$\leq(1.0 \pm 0.3)\times10^{15}$	≤0.005
CH_3CONH_2	0.7	$(1.2 \pm 0.4)\times10^{15}$	0.004	$\leq(3 \pm 1)\times10^{14}$	≤0.0015
CH_2OHCHO	0.4	$(7 \pm 3)\times10^{14}$	0.002	$\leq(4 \pm 1)\times10^{14}$	≤0.002
$OHCH_2CH_2OH$	0.2	$(9 \pm 3)\times10^{15}$	0.03	$\leq(1.0 \pm 0.3)\times10^{15}$	≤0.005
CH_3OH		$(3 \pm 1)\times10^{18}$	10	$(9 \pm 3)\times10^{17}$	4.5
CH_3OCOH		$(9 \pm 3)\times10^{16}$	0.3	$(6 \pm 2)\times10^{16}$	0.3
CH_3COOH		$(1.0 \pm 0.3)\times10^{16}$	0.03	$\leq(3 \pm 1)\times10^{15}$	≤0.015
CH_3CH_2CN		$(3 \pm 1)\times10^{16}$	0.1	$(3 \pm 1)\times10^{16}$	0.15

(a): [D]/[H] = 0.003; from [HDO]/[H_2O] (Neill et al. 2013). (b): [^{16}O]/[^{18}O] = 250; from [^{16}OCS]/[^{18}OCS] (Tercero et al. 2010). (c): [^{12}C]/[^{13}C] = 45 (Tercero et al. 2010). (d): Only the lowest energy conformer, *trans* for $CH_3CH_2NH_2$ and *cis* for CH_3CH_2CHO.

Table B.2. Physical parameters of the considered Orion KL cores

	IRAM 30m	ALMA SV			
		Position A		Position B	
		Comp. 1	Comp. 2	Comp. 1	Comp. 2
v_{LSR} (km s^{-1})	7	8	6	8	5
Δv_{FWHM} (km s^{-1})	5	3	8	3	3
d_{sou} ($''$)	8	3	3	3	3
offset ($''$)	5	...	...	...	...
T_{rot} (K)	150±50	150±50	150±50	150±50	150±50
$N(CH_3NCO)$ (cm^{-2})	$(5 \pm 2)\times10^{15}$	$(5 \pm 2)\times10^{15}$	$(2.5 \pm 0.7)\times10^{15}$	$(2.5 \pm 0.7)\times10^{15}$	$(1.7 \pm 0.5)\times10^{15}$

al. 2015; Tercero et al. 2015). Although there are some remarkable differences in the emission of the latter species, we observe the main core located at the SE of source *n* (at the middle-south of the hot core). Abundant species in the region such as DCN, HDO, and CH_3CN do not show significant emission at the compact ridge.

On the other hand, complex species with nitrogen such as CH_3CH_2CN, CH_2CHCN, and HC_3N, present their emission at the north of the hot core. In addition, emission at the NE of source *I* is more prominent for these species (Guélin et al. 2008; Widicus Weaver & Friedel 2012; Friedel & Widicus Weaver 2012).

Finally, although we do not discuss the emission peaks of CH_3OH (methanol, one of the most abundant species), because they could be affected by opacity effects, we note that methanol is ubiquitous in the region.

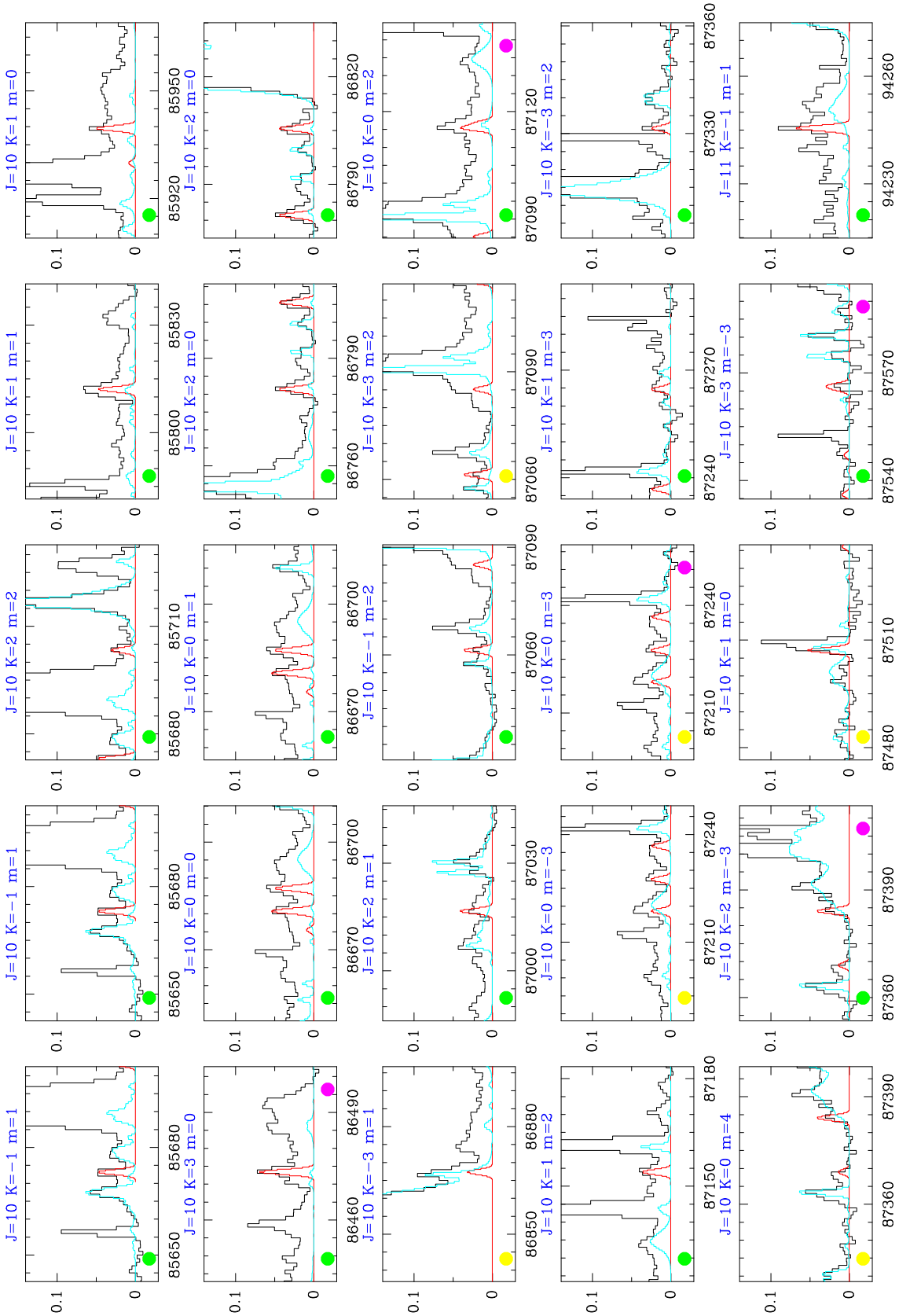

Fig. B.1. Lines of CH_3NCO (here and the next 15 plots) observed with the IRAM 30m telescope and with ALMA (black filled circle in the middle bottom of each panel). The lines are ordered by frequency. The red lines correspond to the CH_3NCO model simulation for both sets of data (see text). The cyan lines correspond to the emission of all modelled molecules to date for the 30m data (see Table B.3). Green filled circles at the bottom left of each panel identify unblended lines, while yellow ones mark lines blended with similar intensity lines from other species. Nevertheless, in the latter case each line profile can be still fitted with a Gaussian profile providing a frequency and intensity for the observed component. Violet filled circles at the bottom right of each panel identify to unresolved doublets. The quantum numbers follow the labelling of Table A.5 except for m=0 for which K_c is not provided (many of these lines are unresolved doublets). The complete set of quantum numbers for m=0 is provided in Table A.6. The units for the intensity scale are Jy/beam for the ALMA data and main beam antenna temperature for the IRAM 30m telescope. A v_{LSR} of +9.0 km s^{-1} is assumed.

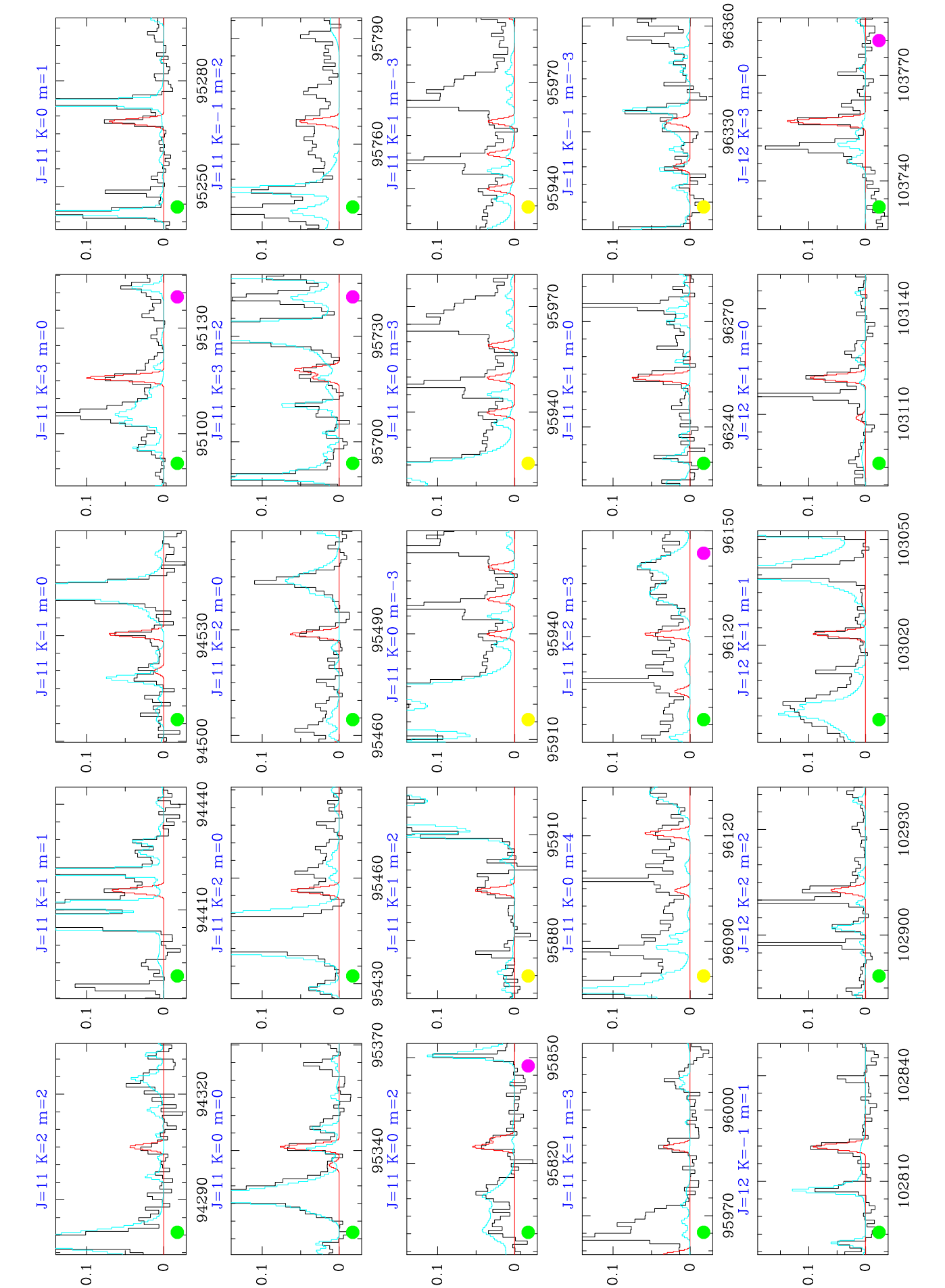
J=11 K=2 m=2
94290
94320
J=11 K=0 m=0
J=11 K=1 m=1
94410
94440
J=11 K=2 m=0
J=11 K=1 m=0
94500
94530
J=11 K=2 m=0
J=11 K=3 m=0
95100
95130
J=11 K=3 m=2
J=11 K=1 m=1
95250
95280
J=11 K=−1 m=2
J=11 K=0 m=1
95340
95370
J=11 K=0 m=2
J=11 K=1 m=2
95430
95460
J=11 K=1 m=2
J=11 K=1 m=0
95460
95490
J=11 K=0 m=−3
J=11 K=1 m=−3
95700
95730
J=11 K=0 m=3
J=11 K=1 m=−3
95760
95790
J=11 K=1 m=−3
J=11 K=2 m=3
95820
95850
J=11 K=1 m=3
J=11 K=0 m=4
95880
95910
J=11 K=0 m=4
J=11 K=2 m=3
95910
95940
J=11 K=2 m=3
J=11 K=1 m=0
95940
95970
J=11 K=1 m=0
J=11 K=−1 m=−3
95940
95970
J=11 K=−1 m=−3
J=12 K=−1 m=1
95970
96000
J=12 K=−1 m=1
J=12 K=2 m=2
96090
96120
J=12 K=2 m=2
J=12 K=1 m=1
96120
96150
J=12 K=1 m=1
J=12 K=1 m=0
96240
96270
J=12 K=1 m=0
J=12 K=3 m=0
96330
96360
J=12 K=3 m=0
102810
102840
102900
102930
103020
103050
103110
103140
103740
103770
0.1
0

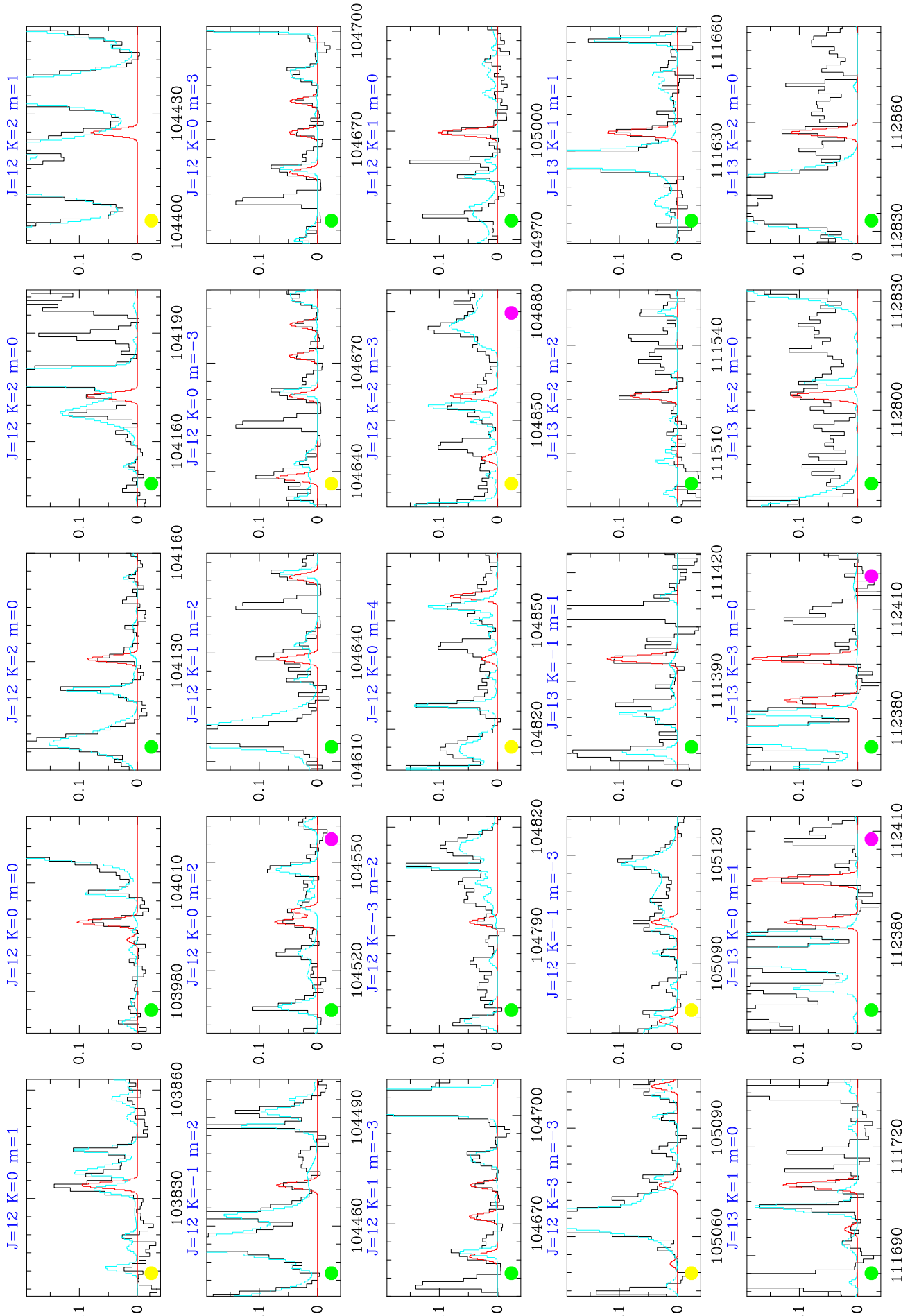
J=12 K=0 m=1
J=12 K=−1 m=2
J=12 K=1 m=−3
J=12 K=3 m=−3
J=13 K=0 m=1
J=13 K=1 m=0
J=12 K=0 m=0
J=12 K=0 m=2
J=12 K=−3 m=2
J=12 K=−1 m=−3
J=13 K=3 m=0
J=13 K=1 m=−1
J=12 K=2 m=0
J=12 K=1 m=2
J=12 K=0 m=4
J=13 K=−1 m=1
J=13 K=2 m=0
J=13 K=2 m=2
J=12 K=2 m=0
J=12 K=0 m=−3
J=12 K=2 m=3
J=13 K=1 m=1
J=13 K=2 m=0
J=12 K=2 m=1
J=12 K=0 m=3
J=12 K=1 m=0
J=13 K=1 m=1
J=13 K=2 m=0

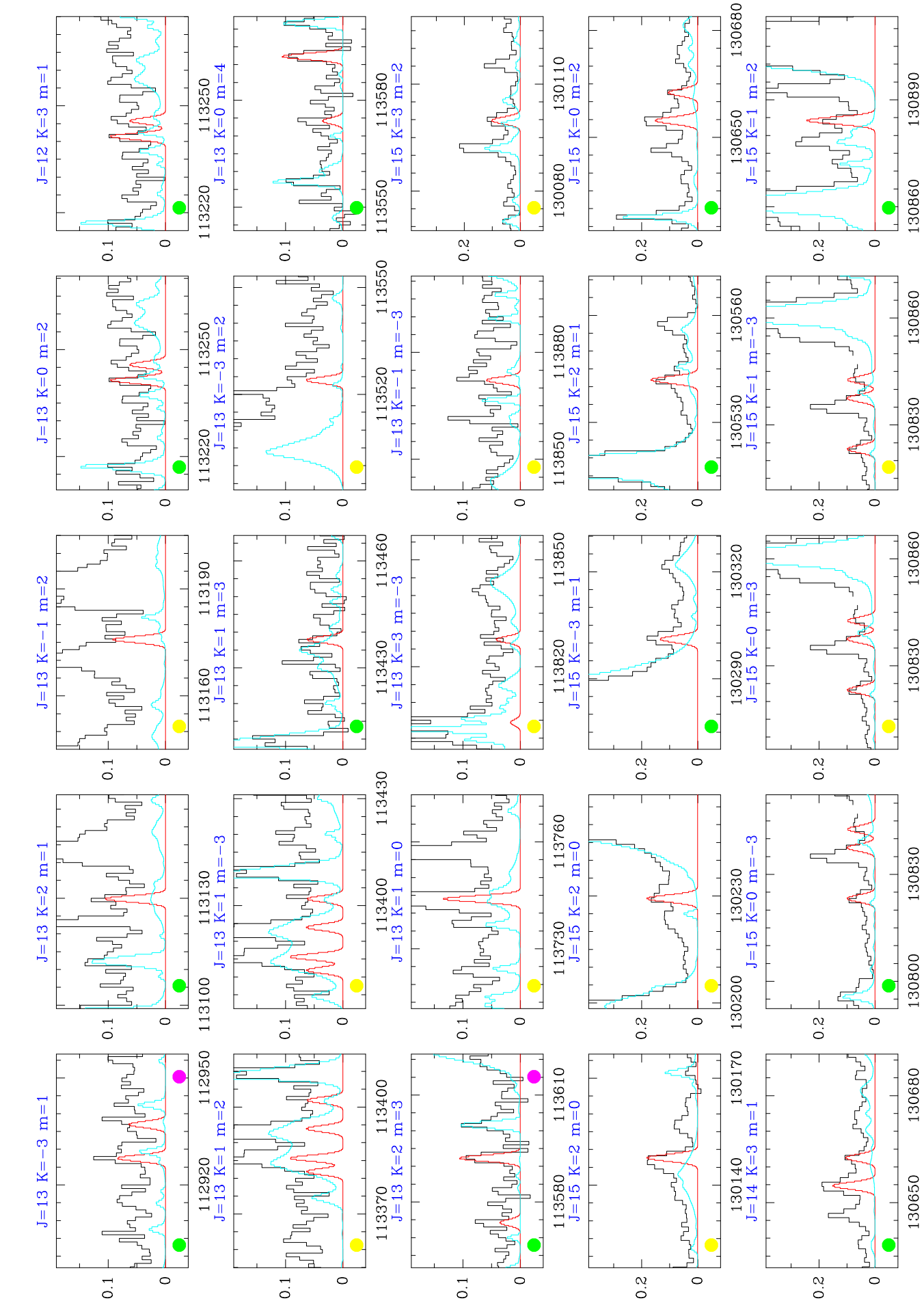
J=13 K=−3 m=1
J=13 K=2 m=1
J=13 K=−1 m=2
J=13 K=0 m=2
J=12 K=3 m=1
112920
J=13 K=1 m=2
113100
J=13 K=1 m=−3
113160
J=13 K=1 m=3
113220
J=13 K=−3 m=2
113220
J=13 K=0 m=4
112950
113130
113190
113250
113250
113370
J=13 K=2 m=3
113400
J=13 K=1 m=0
113430
J=13 K=3 m=−3
113460
113520
J=13 K=−1 m=−3
113550
113550
J=15 K=3 m=2
113580
113580
J=15 K=2 m=0
113730
J=15 K=2 m=0
113760
113820
J=15 K=−3 m=1
113850
113850
J=15 K=2 m=1
113880
130080
J=15 K=0 m=2
130110
130140
J=14 K=3 m=1
130170
130200
J=15 K=0 m=−3
130230
130290
J=15 K=0 m=3
130320
130530
J=15 K=1 m=−3
130560
130650
J=15 K=1 m=2
130680
130650
130800
130830
130860
130890
0.1
0.2
0

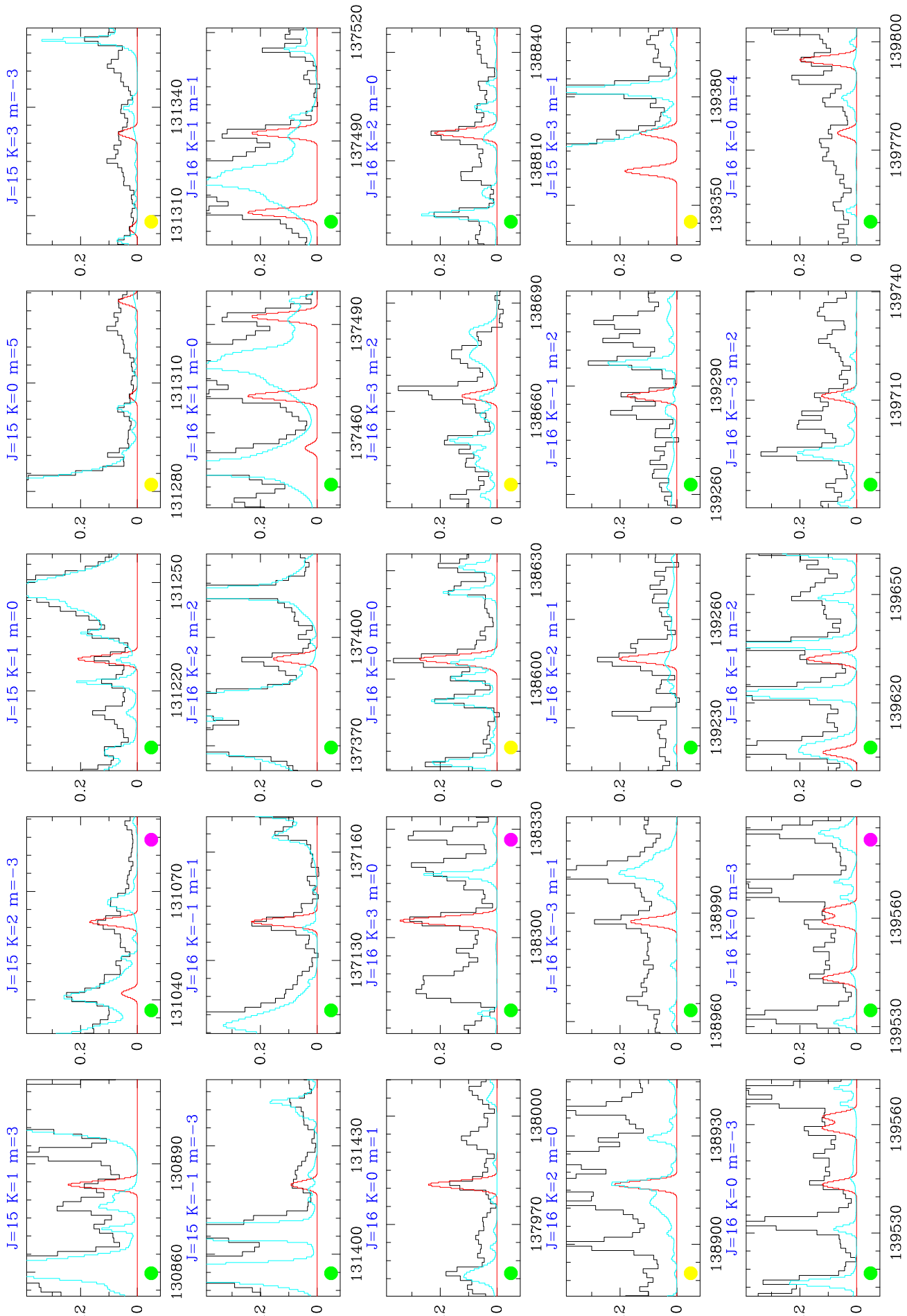
J=15 K=3 m=−3
J=15 K=0 m=5
J=15 K=1 m=0
J=15 K=2 m=−3
J=15 K=1 m=3
130860
J=15 K=−1 m=−3
130890
131310
J=16 K=−1 m=1
131340
131280
J=16 K=1 m=0
131310
131220
J=16 K=2 m=2
131250
131040
J=16 K=−1 m=1
131070
131400
J=16 K=0 m=1
131430
137490
J=16 K=2 m=0
137520
137460
J=16 K=3 m=2
137490
137370
J=16 K=0 m=0
137400
137130
J=16 K=3 m=0
137160
137970
J=16 K=2 m=0
138000
138810
J=15 K=3 m=1
138840
138660
J=16 K=−1 m=2
138690
138600
J=16 K=2 m=1
138630
138300
J=16 K=−3 m=1
138330
138960
J=16 K=0 m=3
138990
139350
J=16 K=0 m=4
139380
139260
J=16 K=−3 m=2
139290
139230
J=16 K=1 m=2
139260
138900
J=16 K=0 m=−3
138930
0.2
0
139530
139560
139710
139740
139620
139650
139530
139560
139770
139800

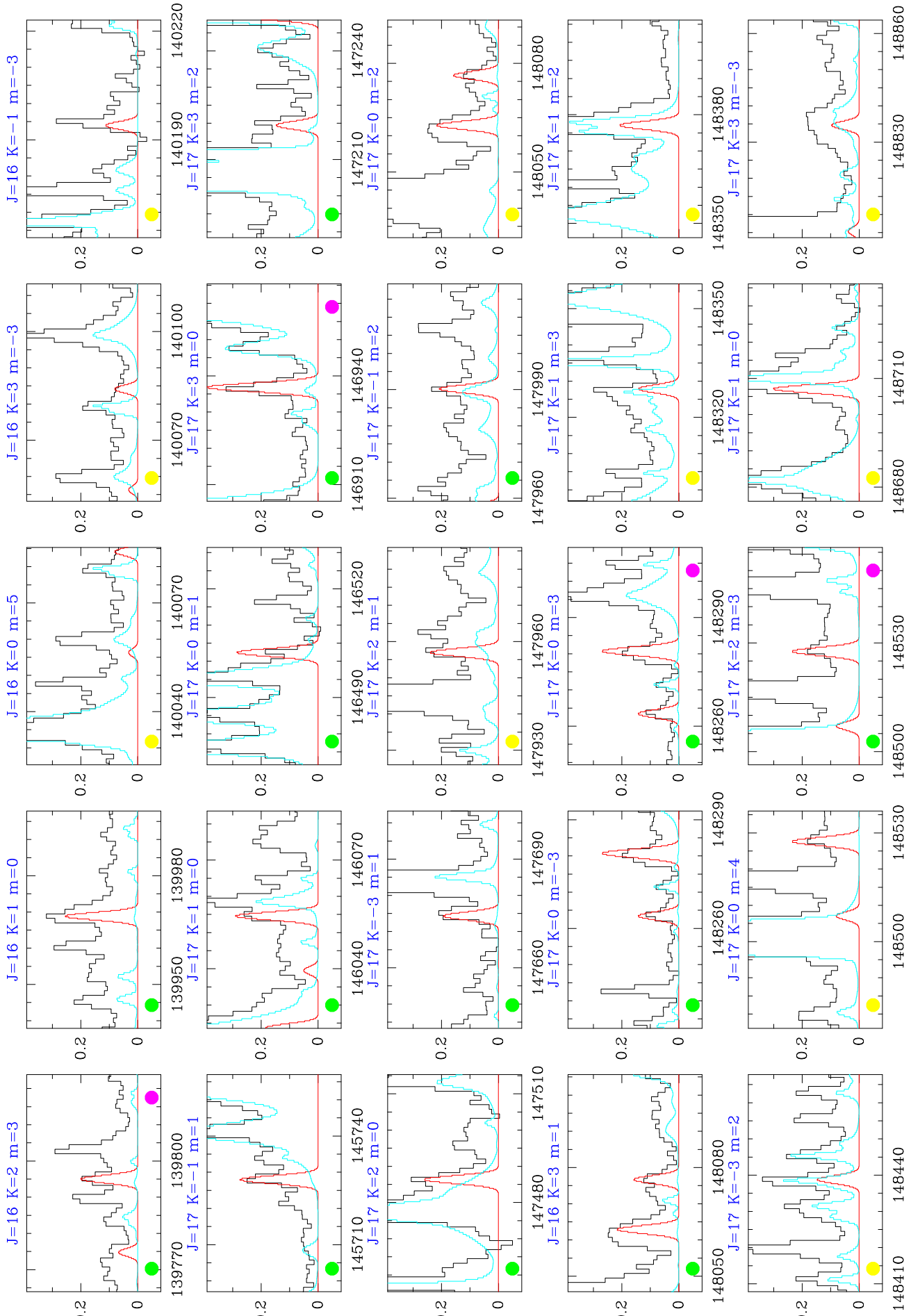
J=16 K=2 m=3
J=16 K=1 m=0
J=16 K=0 m=5
J=16 K=3 m=−3
J=16 K=−1 m=−3
J=17 K=−1 m=1
J=17 K=1 m=0
J=17 K=0 m=1
J=17 K=3 m=0
J=17 K=3 m=2
J=17 K=−3 m=1
J=17 K=2 m=0
J=16 K=3 m=1
J=17 K=0 m=−3
J=17 K=2 m=1
J=17 K=−1 m=2
J=17 K=0 m=2
J=17 K=1 m=3
J=17 K=0 m=3
J=17 K=2 m=3
J=17 K=0 m=4
J=17 K=1 m=2
J=17 K=1 m=0
J=17 K=3 m=−3
J=17 K=−3 m=2
0.2
0

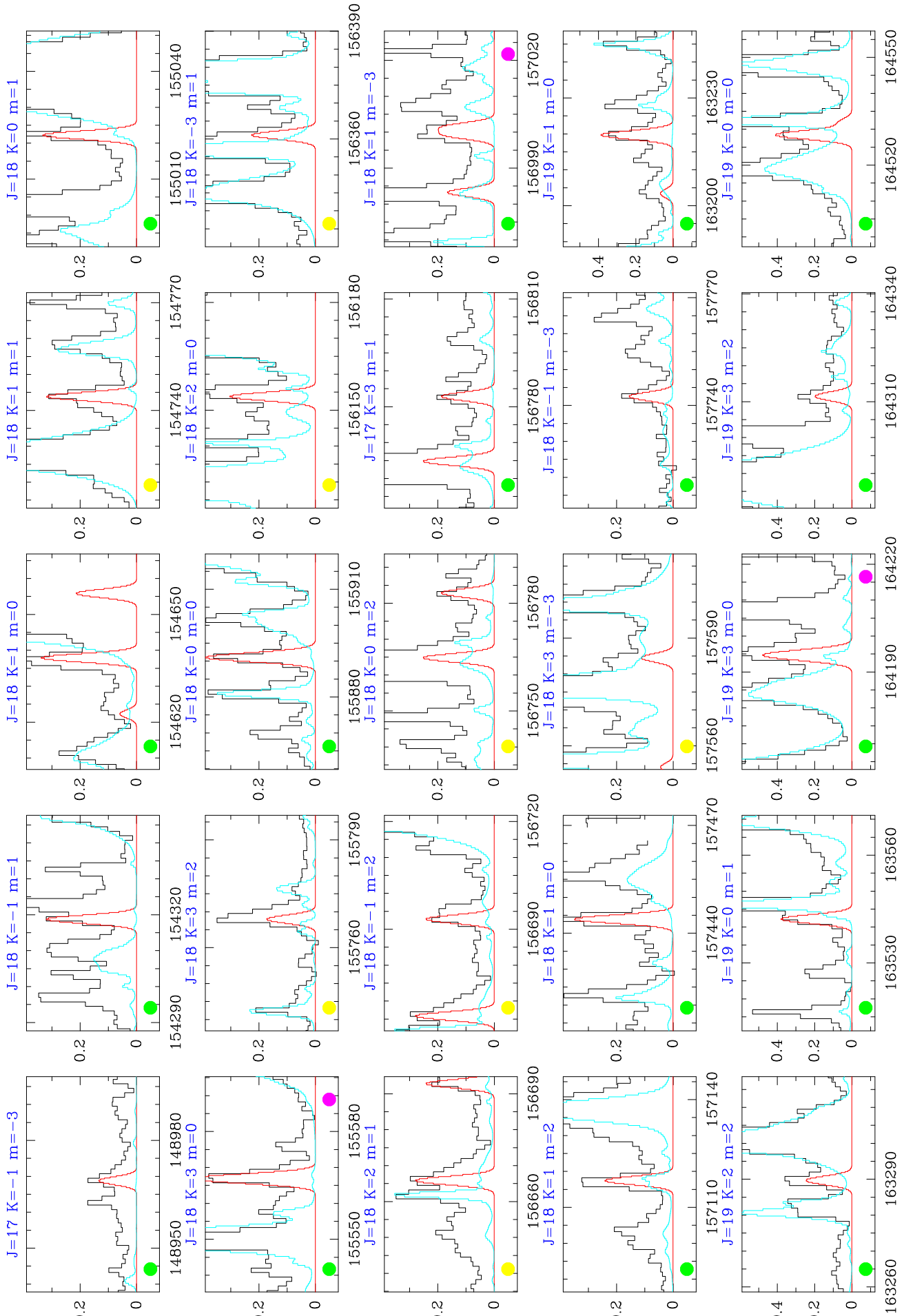
J=17 K=−1 m=−3
148950
148980
J=18 K=3 m=0
J=18 K=−1 m=1
154290
154320
J=18 K=3 m=2
J=18 K=1 m=0
154620
154650
J=18 K=0 m=0
J=18 K=1 m=1
154740
154770
J=18 K=2 m=0
J=18 K=1 m=1
155010
155040
J=18 K=−3 m=1
J=18 K=0 m=0
155550
155580
J=18 K=2 m=1
J=17 K=−1 m=−3
155760
155790
J=18 K=−1 m=2
J=18 K=0 m=2
155880
155910
J=18 K=0 m=2
J=18 K=1 m=−3
156150
156180
J=17 K=3 m=1
J=18 K=1 m=−3
156360
156390
J=18 K=1 m=−3
J=18 K=2 m=1
156660
156690
J=18 K=1 m=2
J=18 K=1 m=0
156690
156720
J=18 K=1 m=0
J=18 K=3 m=−3
156750
156780
J=18 K=3 m=−3
J=18 K=−1 m=−3
156780
156810
J=18 K=−1 m=−3
J=19 K=1 m=0
156990
157020
J=19 K=1 m=0
J=19 K=2 m=2
157110
157140
J=19 K=2 m=2
J=19 K=1 m=1
157440
157470
J=19 K=0 m=1
J=19 K=3 m=0
157560
157590
J=19 K=3 m=0
J=19 K=3 m=2
157740
157770
J=19 K=3 m=2
J=19 K=0 m=0
163200
163230
J=19 K=0 m=0
163260
163290
163530
163560
164190
164220
164310
164340
164520
164550

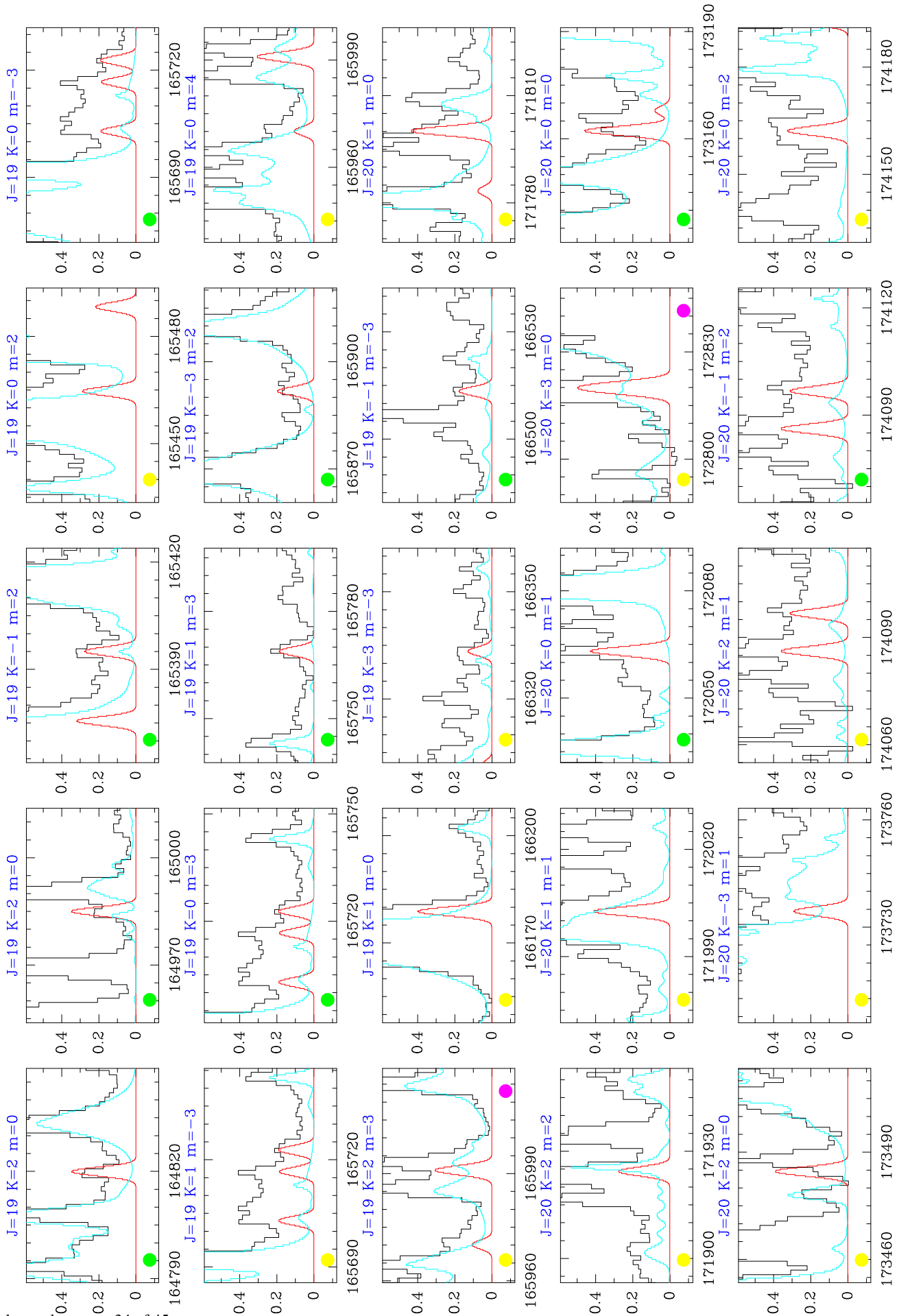
J=19 K=0 m=−3
J=19 K=0 m=2
J=19 K=−1 m=2
J=19 K=2 m=0
J=19 K=2 m=0
J=19 K=−1 m=2
J=19 K=0 m=2
J=19 K=0 m=−3
J=19 K=0 m=4
J=19 K=−3 m=2
J=19 K=1 m=3
J=19 K=0 m=3
J=19 K=1 m=0
J=19 K=3 m=−3
J=19 K=1 m=−3
J=19 K=2 m=3
J=20 K=0 m=0
J=20 K=3 m=0
J=20 K=−1 m=2
J=20 K=2 m=1
J=20 K=0 m=1
J=20 K=1 m=1
J=20 K=−3 m=1
J=20 K=2 m=2
J=20 K=0 m=0
J=20 K=0 m=2
J=20 K=2 m=0
0
0.2
0.4
164790
164820
165690
165720
165960
165990
171780
171810
171900
171930
172800
172830
173160
173190
173460
173490
174150
174180
165690
165720
165960
165990
171780
171810
171900
171930
172800
172830
173160
173190
173460
173490
174150
174180
164970
165000
165390
165420
165750
165780
166320
166350
166170
166200
172050
172080
171990
172020
173730
173760
174060
174090
165450
165480
165870
165900
166500
166530
172800
172830
173160
173190
173460
173490
174090
174120
165450
165480
165870
165900
166500
166530
172800
172830
173160
173190
173460
173490
174090
174120
164970
165000
165390
165420
165750
165780
166320
166350
166170
166200
172050
172080
171990
172020
173730
173760
174060
174090
165690
165720
165960
165990
171780
171810
171900
171930
172800
172830
173160
173190
173460
173490
174150
174180

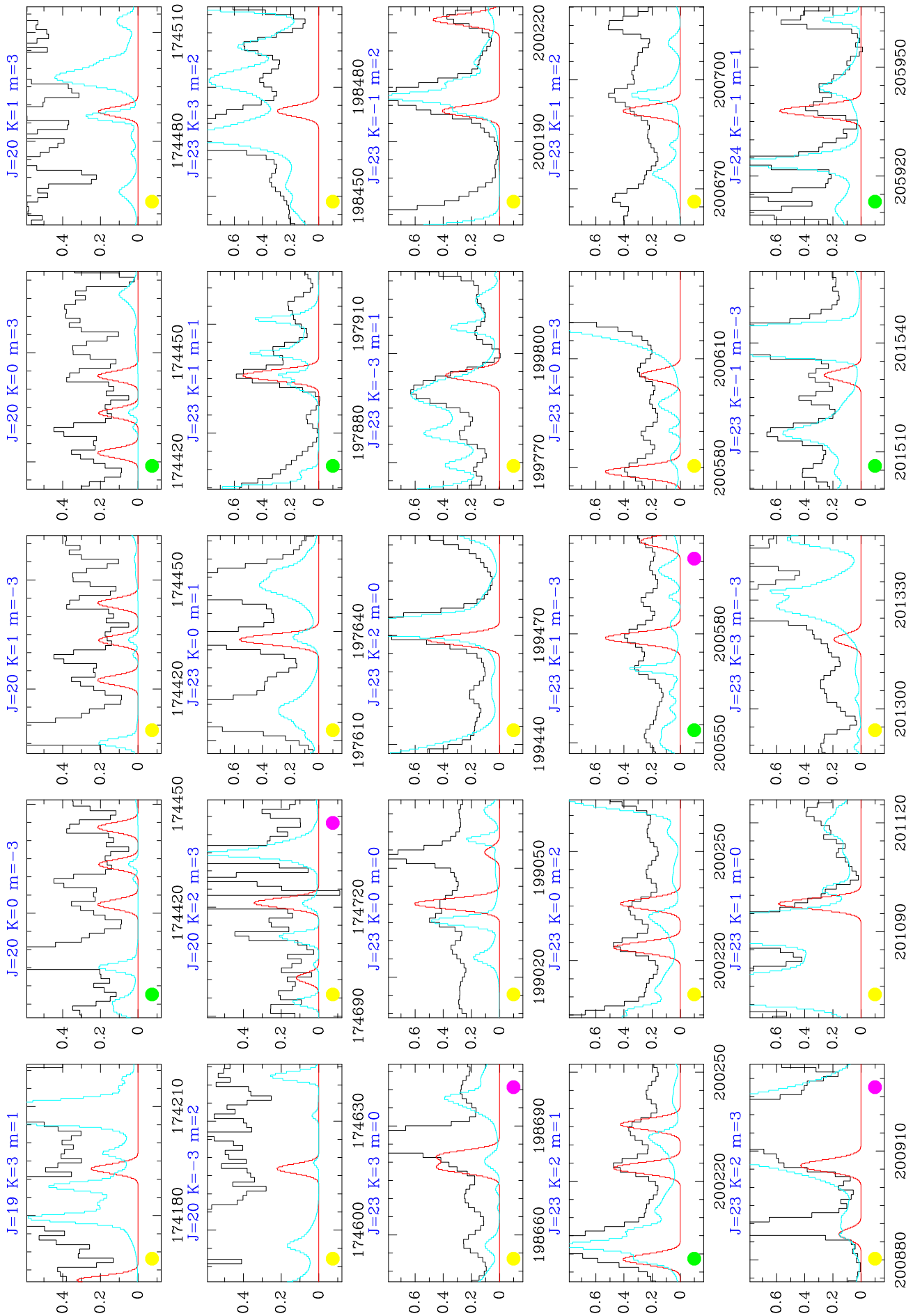
J=19 K=3 m=1
J=20 K=0 m=−3
J=20 K=1 m=−3
J=20 K=0 m=3
J=20 K=1 m=3
174180
J=20 K=−3 m=2
174210
174420
J=20 K=2 m=3
174450
174420
J=23 K=0 m=1
174450
174420
J=23 K=1 m=1
174450
174480
J=23 K=3 m=2
174510
174600
J=23 K=3 m=0
174630
174690
J=23 K=0 m=0
174720
197610
J=23 K=2 m=0
197640
197880
J=23 K=−3 m=1
197910
198450
J=23 K=−1 m=2
198480
198660
J=23 K=2 m=1
198690
199020
J=23 K=0 m=2
199050
199440
J=23 K=1 m=−3
199470
199770
J=23 K=0 m=3
199800
200190
J=23 K=1 m=2
200220
200220
J=23 K=2 m=3
200250
200220
J=23 K=1 m=0
200250
200550
J=23 K=3 m=−3
200580
200580
J=23 K=−1 m=−3
200610
200670
J=24 K=−1 m=1
200700
200880
201090
201300
201510
205920
200910
201120
201330
201540
205950
0
0.2
0.4
0.6

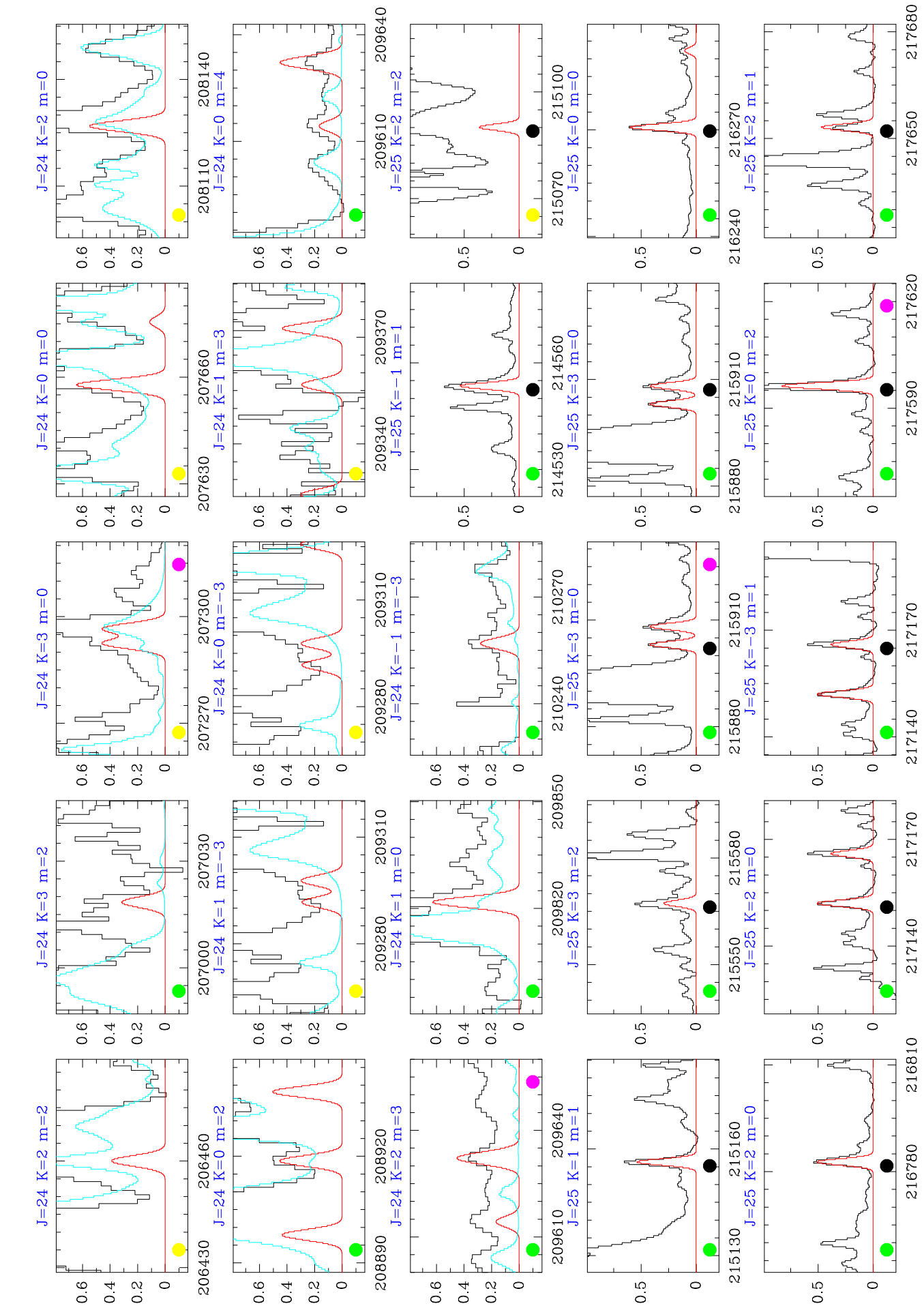
J=24 K=2 m=2
J=24 K=0 m=2
J=24 K=3 m=2
J=24 K=1 m=−3
J=24 K=3 m=0
J=24 K=0 m=−3
J=24 K=0 m=0
J=24 K=1 m=3
J=24 K=2 m=0
J=24 K=0 m=4
J=25 K=1 m=1
J=24 K=2 m=3
J=25 K=3 m=2
J=24 K=1 m=0
J=25 K=3 m=0
J=24 K=−1 m=−3
J=25 K=3 m=0
J=24 K=−1 m=1
J=25 K=2 m=2
J=25 K=2 m=0
J=25 K=−3 m=1
J=25 K=0 m=2
J=25 K=2 m=1
J=25 K=0 m=0

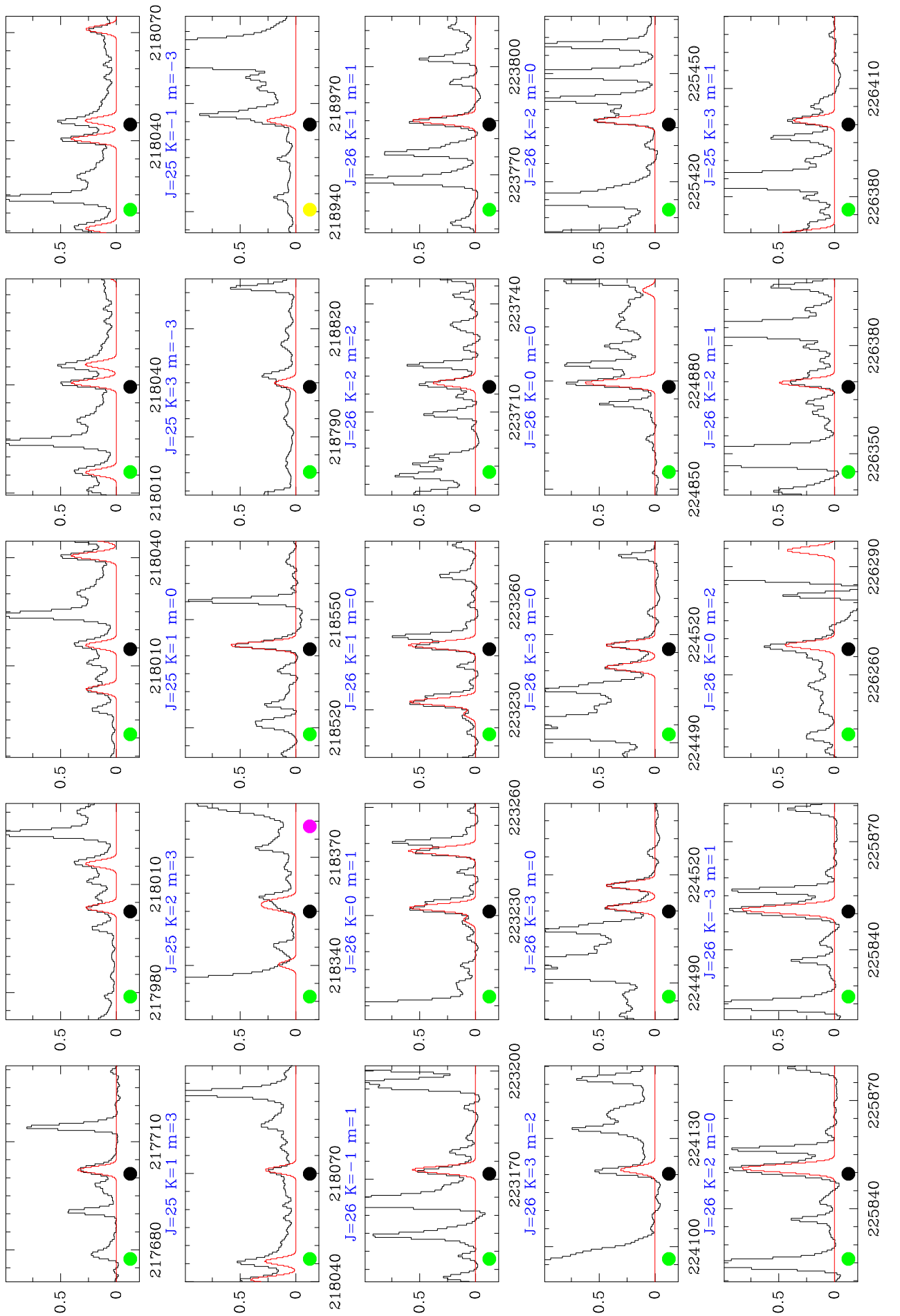
J=24 K=3 m=1
J=25 K=1 m=−3
J=25 K=0 m=−3
J=25 K=1 m=2
J=25 K=0 m=3
217680
217710
217980
218010
218040
218010
218040
218070
224100
224130
224490
224520
224490
224520
224850
224880
225420
225450
223170
223200
223230
223260
223230
223260
223710
223740
223770
223800
218040
218070
218340
218370
218520
218550
218790
218820
218940
218970
225840
225870
225840
225870
226260
226290
226350
226380
226380
226410
0.5
0
J=26 K=3 m=2
J=26 K=−1 m=1
J=25 K=1 m=3
J=26 K=3 m=0
J=26 K=0 m=1
J=25 K=2 m=3
J=26 K=3 m=0
J=26 K=1 m=0
J=25 K=1 m=0
J=26 K=0 m=0
J=26 K=2 m=2
J=26 K=1 m=1
J=25 K=3 m=−3
J=26 K=2 m=0
J=25 K=−1 m=−3
J=25 K=0 m=3
J=26 K=2 m=0
J=26 K=−3 m=1
J=26 K=0 m=2
J=26 K=2 m=1
J=25 K=3 m=1

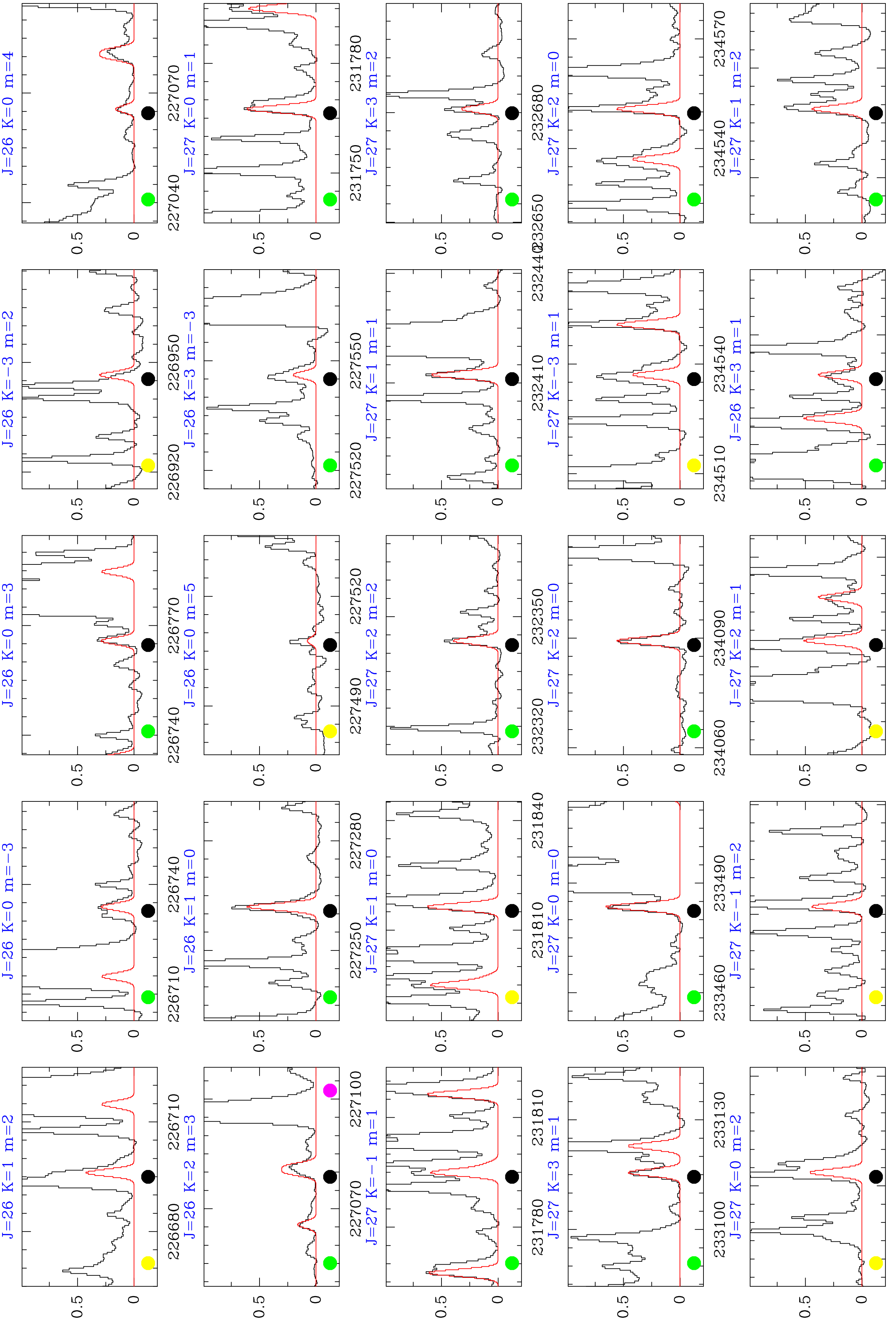
J=26 K=0 m=4
J=26 K=−3 m=2
J=26 K=0 m=3
J=26 K=0 m=−3
J=26 K=1 m=2
J=27 K=0 m=1
J=26 K=3 m=−3
J=26 K=0 m=5
J=26 K=1 m=0
J=26 K=2 m=3
J=27 K=3 m=2
J=27 K=1 m=1
J=27 K=2 m=2
J=27 K=1 m=0
J=27 K=−1 m=1
J=27 K=2 m=0
J=27 K=−3 m=1
J=27 K=2 m=0
J=27 K=0 m=0
J=27 K=3 m=1
J=27 K=1 m=2
J=26 K=3 m=1
J=27 K=2 m=1
J=27 K=−1 m=2
J=27 K=0 m=2

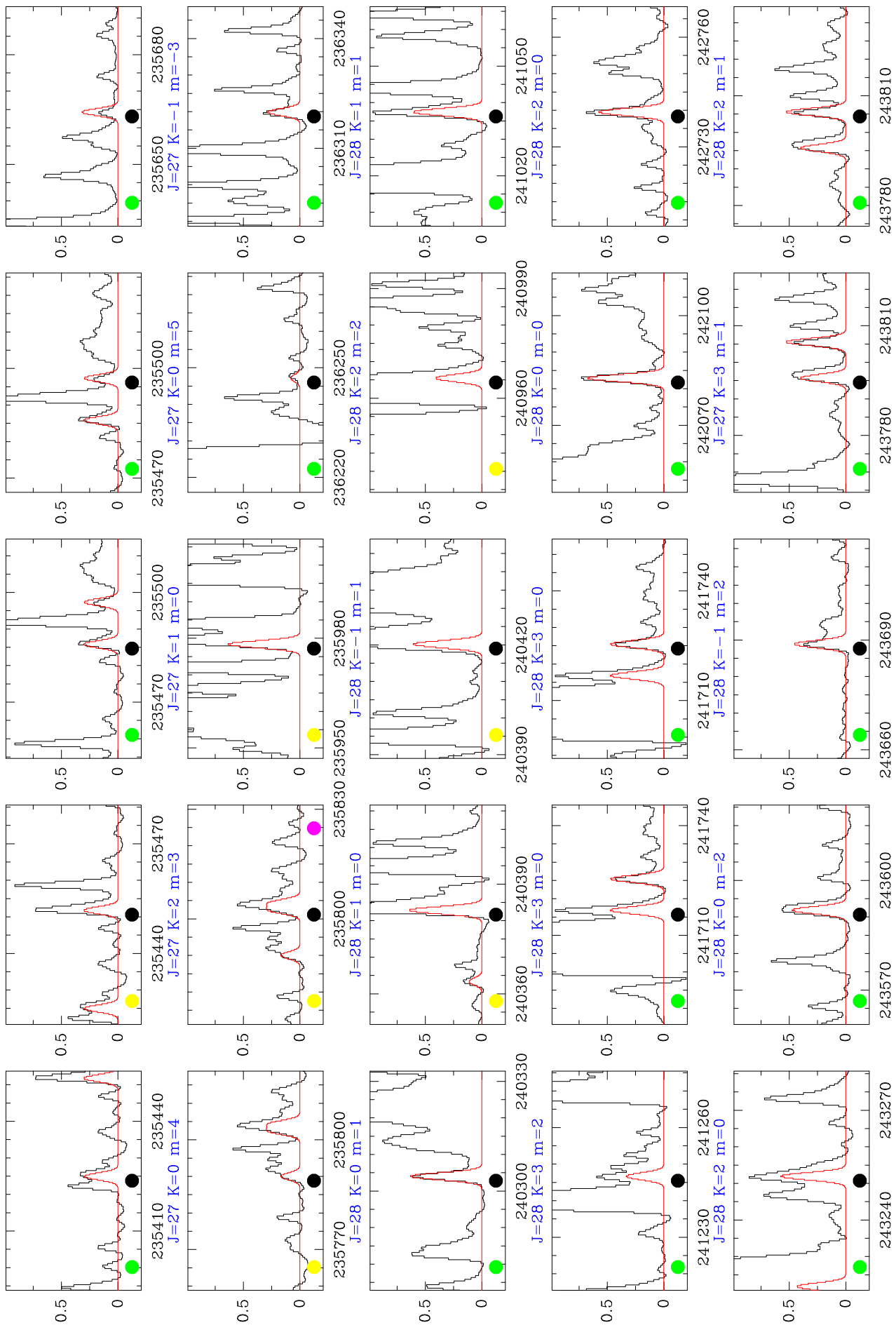
J=27 K=−3 m=2
J=27 K=−1 m=−3
J=28 K=1 m=1
J=28 K=2 m=0
J=28 K=2 m=1
J=27 K=1 m=3
J=27 K=0 m=5
J=28 K=2 m=2
J=28 K=0 m=0
J=27 K=3 m=1
J=27 K=0 m=3
J=27 K=1 m=0
J=28 K=−1 m=1
J=28 K=3 m=0
J=28 K=−1 m=2
J=27 K=0 m=−3
J=27 K=2 m=3
J=28 K=1 m=0
J=28 K=3 m=0
J=28 K=0 m=2
J=27 K=1 m=−3
J=27 K=0 m=4
J=28 K=0 m=1
J=28 K=3 m=2
J=28 K=2 m=0
0
0.5

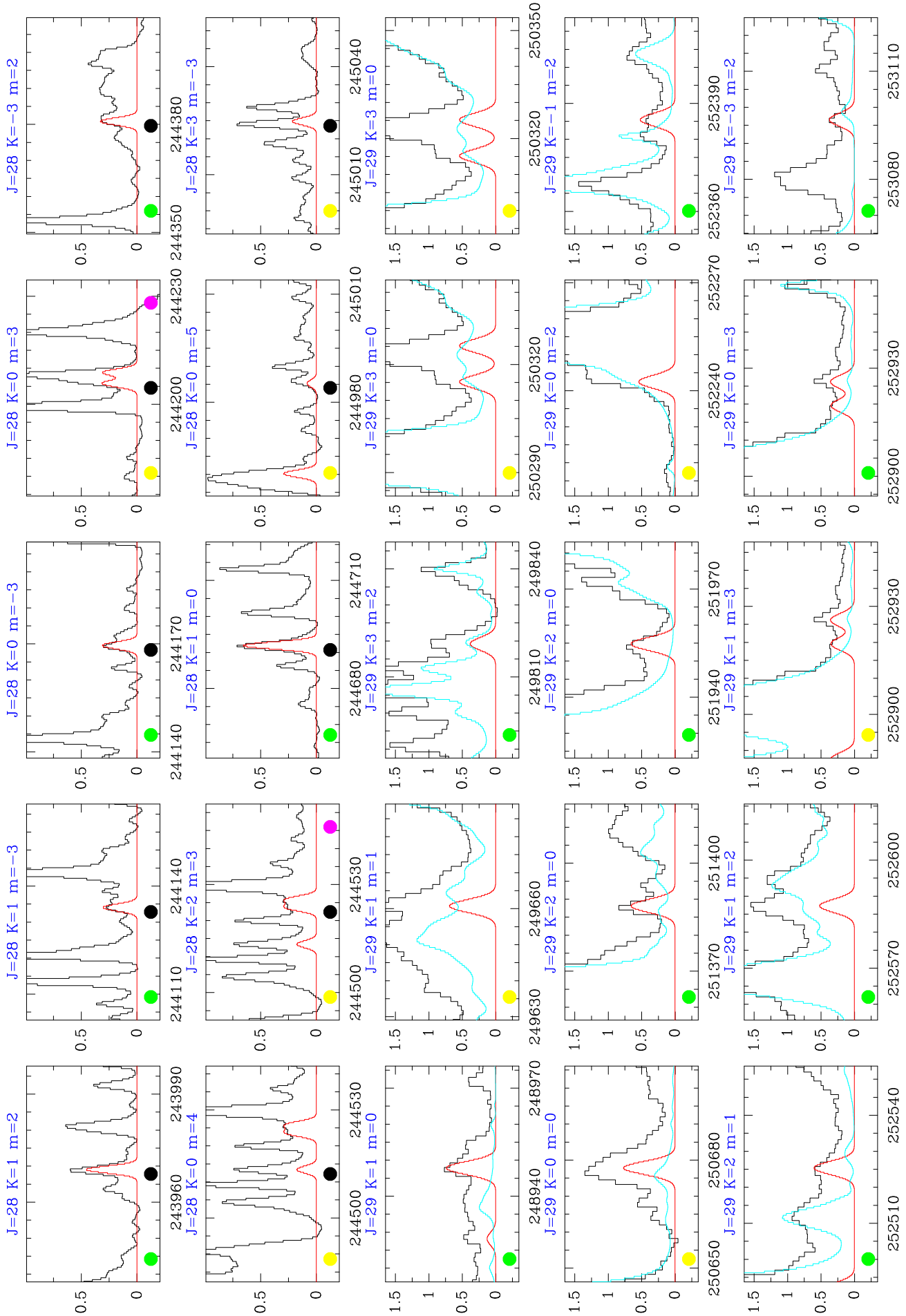
J=28 K=1 m=2
243960
J=28 K=0 m=4
243990
244500
J=29 K=1 m=0
244530
248940
J=29 K=0 m=0
248970
250650
J=29 K=2 m=1
250680
252510
252540
J=28 K=1 m=−3
244110
J=28 K=2 m=3
244140
244500
J=29 K=1 m=1
244530
249630
J=29 K=2 m=0
249660
251370
J=29 K=1 m=2
251400
252570
252600
J=28 K=0 m=−3
244140
J=28 K=1 m=0
244170
244680
J=29 K=3 m=2
244710
249810
J=29 K=2 m=0
249840
251940
J=29 K=1 m=3
251970
252900
252930
J=28 K=0 m=3
244200
J=28 K=0 m=5
244230
244980
J=29 K=3 m=0
245010
250290
J=29 K=0 m=2
250320
252240
J=29 K=0 m=3
252270
252900
252930
J=28 K=−3 m=2
244350
J=28 K=3 m=−3
244380
245010
J=29 K=3 m=0
245040
250320
J=29 K=−1 m=2
250350
252360
J=29 K=−3 m=2
252390
253080
253110

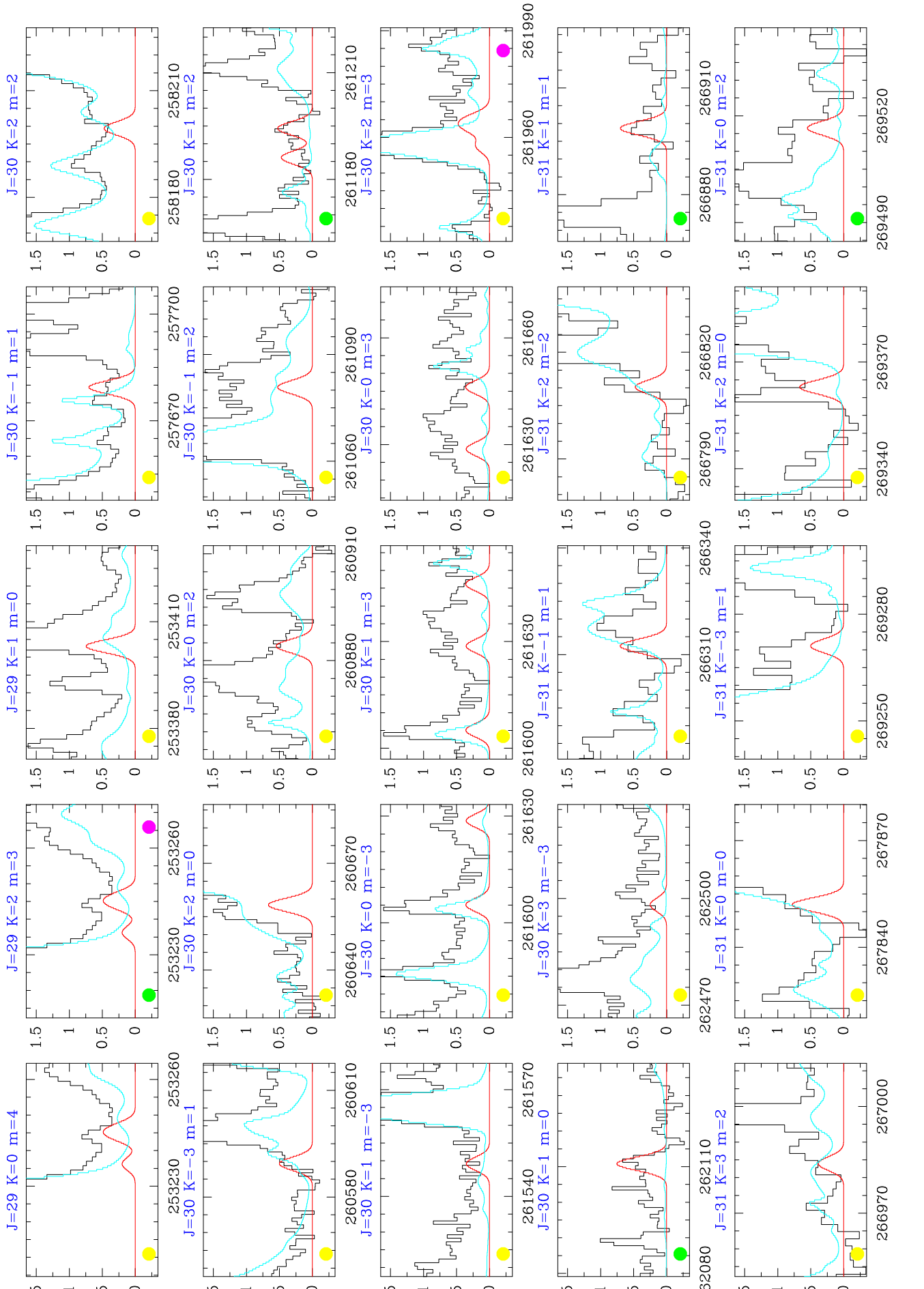
J=29 K=0 m=4
J=29 K=1 m=0
J=29 K=2 m=3
J=30 K=−1 m=1
J=30 K=2 m=2
J=30 K=−3 m=1
J=30 K=1 m=2
J=30 K=−1 m=2
J=30 K=0 m=3
J=30 K=2 m=3
J=30 K=1 m=−3
J=30 K=0 m=2
J=30 K=2 m=0
J=30 K=−1 m=3
J=30 K=1 m=3
J=30 K=3 m=−3
J=31 K=3 m=2
J=31 K=0 m=2
J=31 K=2 m=0
J=31 K=1 m=1
J=31 K=−1 m=1
J=31 K=−3 m=1
J=31 K=0 m=0
J=31 K=2 m=2
J=31 K=1 m=0
J=31 K=−1 m=0
J=31 K=−3 m=0
J=31 K=1 m=−3
J=31 K=−1 m=−3
J=31 K=−3 m=−3
J=31 K=3 m=3
J=31 K=2 m=3
J=31 K=1 m=3
J=31 K=0 m=3
J=31 K=−1 m=3
J=31 K=−3 m=3
J=31 K=3 m=4
J=31 K=2 m=4
J=31 K=1 m=4
J=31 K=0 m=4
J=31 K=−1 m=4
J=31 K=−3 m=4
J=31 K=3 m=5
J=31 K=2 m=5
J=31 K=1 m=5
J=31 K=0 m=5
J=31 K=−1 m=5
J=31 K=−3 m=5
J=32 K=3 m=3
J=32 K=2 m=3
J=32 K=1 m=3
J=32 K=0 m=3
J=32 K=−1 m=3
J=32 K=−3 m=3
J=32 K=3 m=4
J=32 K=2 m=4
J=32 K=1 m=4
J=32 K=0 m=4
J=32 K=−1 m=4
J=32 K=−3 m=4
J=32 K=3 m=5
J=32 K=2 m=5
J=32 K=1 m=5
J=32 K=0 m=5
J=32 K=−1 m=5
J=32 K=−3 m=5
J=33 K=3 m=3
J=33 K=2 m=3
J=33 K=1 m=3
J=33 K=0 m=3
J=33 K=−1 m=3
J=33 K=−3 m=3
J=33 K=3 m=4
J=33 K=2 m=4
J=33 K=1 m=4
J=33 K=0 m=4
J=33 K=−1 m=4
J=33 K=−3 m=4
J=33 K=3 m=5
J=33 K=2 m=5
J=33 K=1 m=5
J=33 K=0 m=5
J=33 K=−1 m=5
J=33 K=−3 m=5
J=34 K=3 m=3
J=34 K=2 m=3
J=34 K=1 m=3
J=34 K=0 m=3
J=34 K=−1 m=3
J=34 K=−3 m=3
J=34 K=3 m=4
J=34 K=2 m=4
J=34 K=1 m=4
J=34 K=0 m=4
J=34 K=−1 m=4
J=34 K=−3 m=4
J=34 K=3 m=5
J=34 K=2 m=5
J=34 K=1 m=5
J=34 K=0 m=5
J=34 K=−1 m=5
J=34 K=−3 m=5
J=35 K=3 m=3
J=35 K=2 m=3
J=35 K=1 m=3
J=35 K=0 m=3
J=35 K=−1 m=3
J=35 K=−3 m=3
J=35 K=3 m=4
J=35 K=2 m=4
J=35 K=1 m=4
J=35 K=0 m=4
J=35 K=−1 m=4
J=35 K=−3 m=4
J=35 K=3 m=5
J=35 K=2 m=5
J=35 K=1 m=5
J=35 K=0 m=5
J=35 K=−1 m=5
J=35 K=−3 m=5
J=36 K=3 m=3
J=36 K=2 m=3
J=36 K=1 m=3
J=36 K=0 m=3
J=36 K=−1 m=3
J=36 K=−3 m=3
J=36 K=3 m=4
J=36 K=2 m=4
J=36 K=1 m=4
J=36 K=0 m=4
J=36 K=−1 m=4
J=36 K=−3 m=4
J=36 K=3 m=5
J=36 K=2 m=5
J=36 K=1 m=5
J=36 K=0 m=5
J=36 K=−1 m=5
J=36 K=−3 m=5
J=37 K=3 m=3
J=37 K=2 m=3
J=37 K=1 m=3
J=37 K=0 m=3
J=37 K=−1 m=3
J=37 K=−3 m=3
J=37 K=3 m=4
J=37 K=2 m=4
J=37 K=1 m=4
J=37 K=0 m=4
J=37 K=−1 m=4
J=37 K=−3 m=4
J=37 K=3 m=5
J=37 K=2 m=5
J=37 K=1 m=5
J=37 K=0 m=5
J=37 K=−1 m=5
J=37 K=−3 m=5
J=38 K=3 m=3
J=38 K=2 m=3
J=38 K=1 m=3
J=38 K=0 m=3
J=38 K=−1 m=3
J=38 K=−3 m=3
J=38 K=3 m=4
J=38 K=2 m=4
J=38 K=1 m=4
J=38 K=0 m=4
J=38 K=−1 m=4
J=38 K=−3 m=4
J=38 K=3 m=5
J=38 K=2 m=5
J=38 K=1 m=5
J=38 K=0 m=5
J=38 K=−1 m=5
J=38 K=−3 m=5
J=39 K=3 m=3
J=39 K=2 m=3
J=39 K=1 m=3
J=39 K=0 m=3
J=39 K=−1 m=3
J=39 K=−3 m=3
J=39 K=3 m=4
J=39 K=2 m=4
J=39 K=1 m=4
J=39 K=0 m=4
J=39 K=−1 m=4
J=39 K=−3 m=4
J=39 K=3 m=5
J=39 K=2 m=5
J=39 K=1 m=5
J=39 K=0 m=5
J=39 K=−1 m=5
J=39 K=−3 m=5
J=40 K=3 m=3
J=40 K=2 m=3
J=40 K=1 m=3
J=40 K=0 m=3
J=40 K=−1 m=3
J=40 K=−3 m=3
J=40 K=3 m=4
J=40 K=2 m=4
J=40 K=1 m=4
J=40 K=0 m=4
J=40 K=−1 m=4
J=40 K=−3 m=4
J=40 K=3 m=5
J=40 K=2 m=5
J=40 K=1 m=5
J=40 K=0 m=5
J=40 K=−1 m=5
J=40 K=−3 m=5

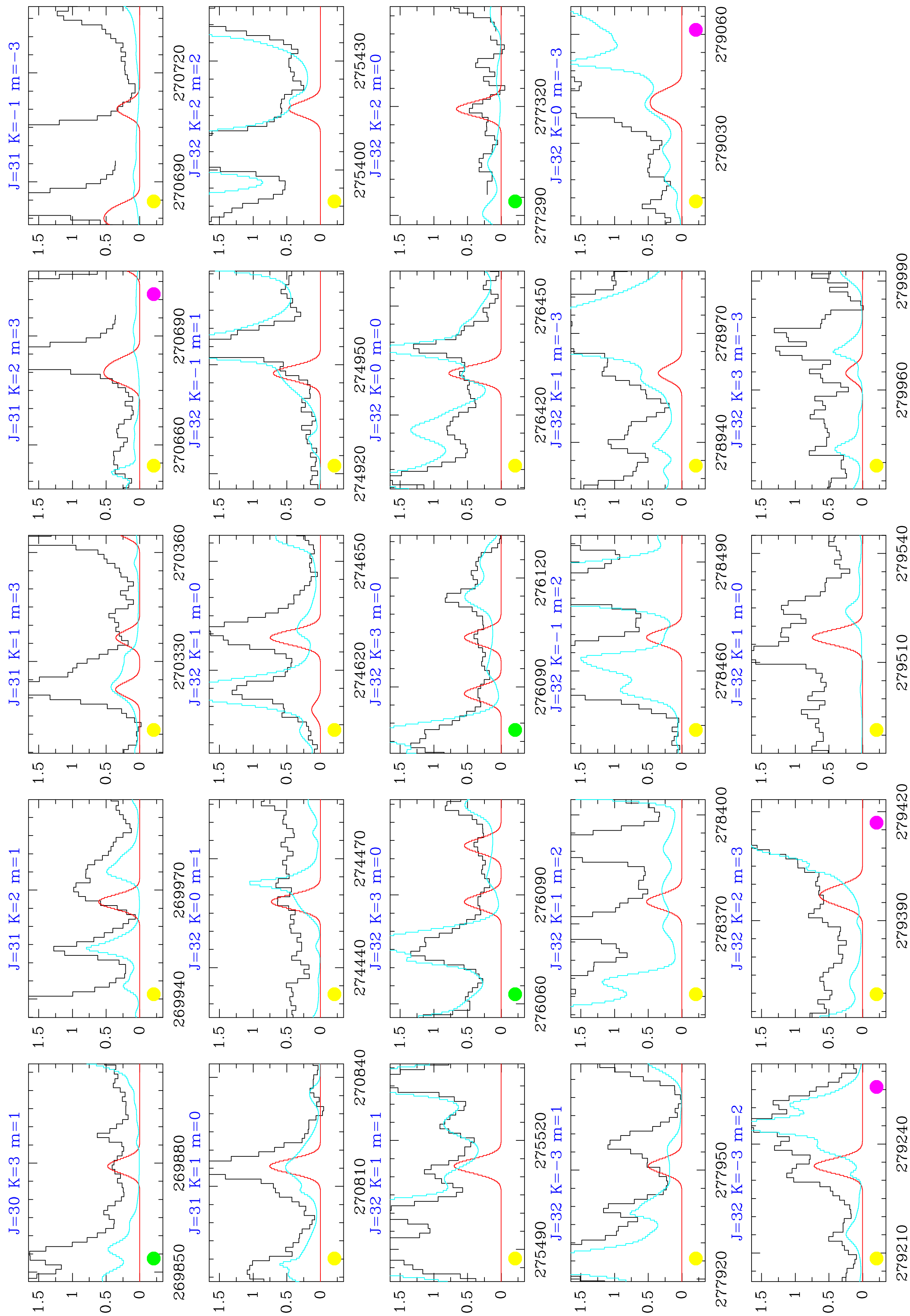
J=30 K=3 m=1
J=31 K=2 m=1
J=31 K=1 m=3
J=31 K=2 m=3
J=31 K=−1 m=−3
J=31 K=1 m=0
J=32 K=0 m=1
J=32 K=1 m=0
J=32 K=−1 m=1
J=32 K=2 m=2
J=32 K=1 m=1
J=32 K=3 m=0
J=32 K=3 m=0
J=32 K=0 m=0
J=32 K=2 m=0
J=32 K=−3 m=1
J=32 K=1 m=2
J=32 K=−1 m=2
J=32 K=1 m=−3
J=32 K=0 m=−3
J=32 K=−3 m=2
J=32 K=2 m=3
J=32 K=1 m=0
J=32 K=3 m=−3

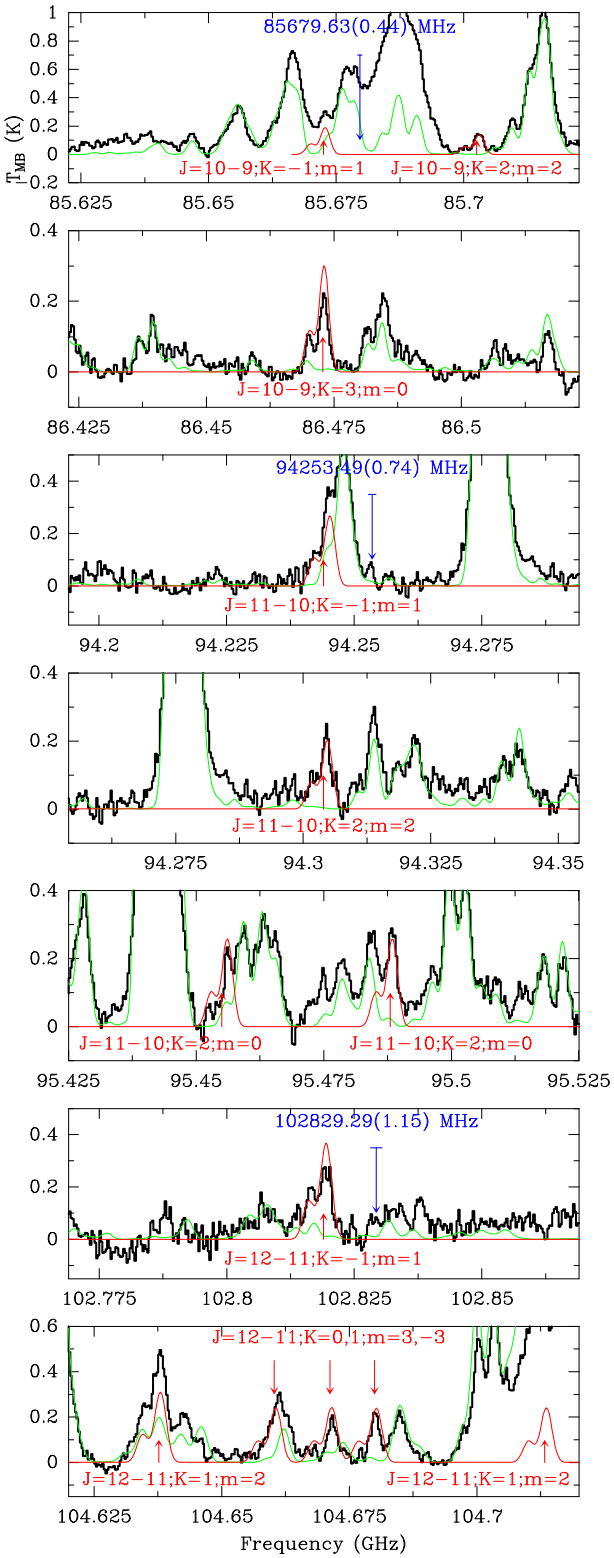

Fig. B.2. Selected lines of CH_3NCO in Sgr B2(N) at 3 mm. Observed data (black histogram spectrum) and total model of the source (green curve) are from Belloche et al. (2013). Our best model for CH_3NCO is given by the red line. Frequencies given by Halfen et al. (2015) with their uncertainty are indicated by the blue arrows and lines. A v_{LSR} of +64.0 km s^{-1} is assumed.

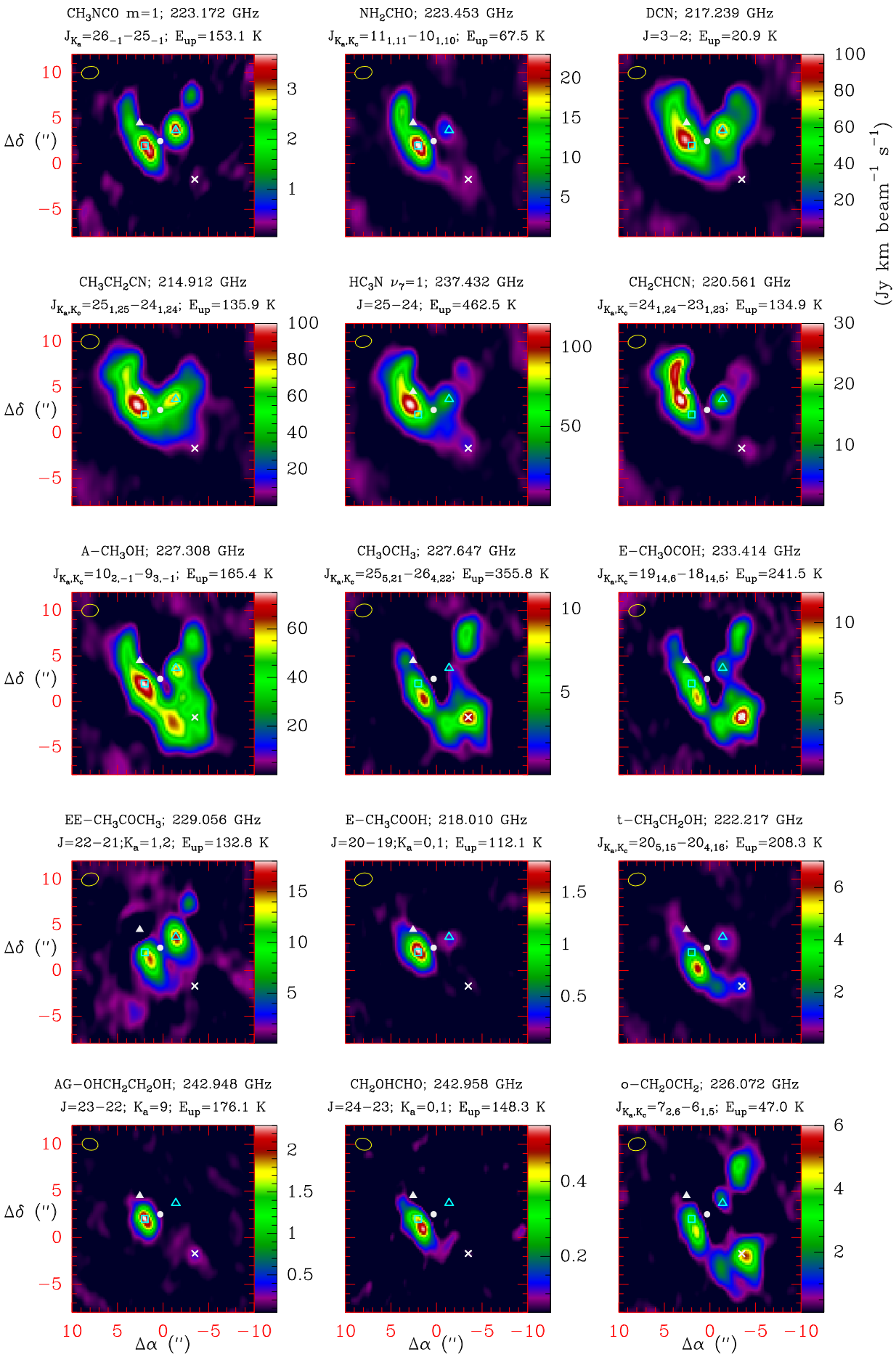

Fig. B.3. Spatial distribution of selected molecules from the ALMA data of Orion between 213−247 GHz (see text).

Table B.3. Model for the IRAM 30m data based on previously analysed molecular species

Reference	Studied species	Notes
Tercero et al. (2010)†	OCS, CS, H_2CS, HCS^+, CCS, CCCS	(b) (c)
Tercero et al. (2011)†	SiO, SiS	(b) (c)
Daly et al. (2013)†	CH_3CH_2CN	(a) (b) (c)
Esplugues et al. (2013a)†	SO, SO_2	(b) (c)
Esplugues et al. (2013b)†	HC_3N, HC_5N	(b) (c) (d)
López et al. (2014)†	CH_2CHCN	(a) (b) (c)
Marcelino et al. in prep.†	HCN, HNC, HCO^+	(b) (c) (d) (e)
Demyk et al. (2007)	^{13}C-CH_3CH_2CN	(a) (c)
Margulès et al. (2009)	$CH_3CH_2C^{15}N$, CH_3CHDCN, CH_2DCH_2CN	(a) (c)
Carvajal et al. (2009)	^{13}C-$HCOOCH_3$	(a) (c)
Marcelino et al. (2009)	HNCO	(c)
Margulès et al. (2010)	$DCOOCH_3$	(a) (c)
Tercero et al. (2012)	^{18}O-$HCOOCH_3$	(a) (c)
Motiyenko et al. (2012)	NH_2CHO, NH_2CHO v_{12}=1	(a) (c)
Coudert et al. (2013)	$HCOOCH_2D$	(a) (c)
Tercero et al. (2013)	CH_3COOCH_3, CH_3CH_2OCOH	(a) (c)
Cernicharo et al. (2013)	NH_3D^+	(a) (c)
Kolesniková et al. (2013)	c-C_6H_5OH (not detected)	(a) (c)
Haykal et al. (2013)	CH_2CHCH_2NC (not detected)	(a) (c)
Bell et al. (2014)	CH_3CN	(b) (c)
Kolesniková et al. (2014)	CH_3CH_2SH, CH_3SH, CH_3OH, $^{13}CH_3OH$, CH_3CH_2OH	(a) (c)
Haykal et al. (2014)	^{13}C-$HCOOCH_3$ v_t=1	(a) (c)
Tercero et al. (2015)	$CH_3CH_2OCH_3$	(c) (e)
Kolesniková et al. (2015)	$CH_3COOCHCH_2$ (not detected)	(a) (c) (e)
Alonso et al. (2015)	$CH_2CHCOOH$ (not detected)	(a) (c) (e)
López et al. in prep.	$HCOOCH_3$ v_t=0,1,2, CH_3COOH v_t=0,1,2, CH_2OHCHO	(c) (e)
In progress	CH_2OCH_2, AG-$OHCH_2CH_2OH$	(c)
In progress	^{13}C-CH_3CN, CH_3CN v_8=1	(c)
In progress	CH_3OCH_3, CH_3COCH_3, $H_2{}^{13}CO$	(c)

†: In this analysis we have include all isotopologues and vibrational excited states of the molecule. (a) - Papers in collaboration with spectroscopists. (b) - Papers dividing the analysis of the Orion surveys in different families of molecules. (c) - Papers based on the IRAM 30m 1D-survey (Tercero et al. 2010) and/or 2D-survey (Marcelino et al. in prep.). (d) - Papers based on Herschel/HIFI data. (e) - Papers based on ALMA SV data.